An Overview of Gadolinium-Based Oxide and Oxysulfide Particles: Synthesis, Properties, and Biomedical Applications

Benita Ortega-Berlanga [1,2]**, Lourdes Betancourt-Mendiola** [1,2] **, César del Angel-Olarte** [1,2]**,
Luis Hernández-Adame** [3]**, Sergio Rosales-Mendoza** [1,2] **and Gabriela Palestino** [1,2,*]

1   Facultad de Ciencias Químicas, Universidad Autónoma de San Luis Potosí, Av. Dr. Manuel Nava 6,
    San Luis Potosí 78210, Mexico; benita.orbe@gmail.com (B.O.-B.); lourdes.betancourt@uaslp.mx (L.B.-M.);
    cesar.manuel.delangel@gmail.com (C.d.A.-O.); rosales.s@uaslp.mx (S.R.-M.)
2   Sección de Biotecnología, Centro de Investigación en Ciencias de la Salud y Biomedicina, Universidad
    Autónoma de San Luis Potosí, Av. Sierra Leona 550, Lomas 2a Sección, San Luis Potosí 78210, Mexico
3   CONACYT-Centro de Investigaciones Biológicas del Noroeste (CIBNOR), Instituto Politécnico Nacional 195,
    Playa Palo de Santa Rita Sur, La Paz 23090, Mexico; ladame@cibnor.mx
*   Correspondence: palestinogabriela@uaslp.mx; Tel.: +52-444-826-2300 (ext. 6525)

Abstract: In the last decade, the publications presenting novel physical and chemical aspects of gadolinium-based oxide (Gd_2O_3) and oxysulfide (Gd_2O_2S) particles in the micro- or nano-scale have increased, mainly stimulated by the exciting applications of these materials in the biomedical field. Their optical properties, related to down and upconversion phenomena and the ability to functionalize their surface, make them attractive for developing new probes for selective targeting and emergent bioimaging techniques, either for biomolecule labeling or theranostics. Moreover, recent reports have shown interesting optical behavior of these systems influenced by the synthesis methods, dopant amount and type, particle shape and size, and surface functionality. Hence, this review presents a compilation of the latest works focused on evaluating the optical properties of Gd_2O_3 and Gd_2O_2S particles as a function of their physicochemical and morphological properties; and also on their novel applications as MRI contrast agents and drug delivery nanovehicles, discussed along with their administration routes, biodistribution, cytotoxicity, and clearance mechanisms. Perspectives for this field are also identified and discussed.

Keywords: Gd_2O_3; Gd_2O_2S; nanoparticles; optical properties; biological applications

1. Introduction

Research into lanthanide-based materials emerged in the early 1990s with the development of high-efficiency materials for optics: new fiber amplifiers, stable solid-state lasers, sensors, devices with upconversion, devices with non-linear responses, among others [1]. At present, the interest in investigating Gd_2O_3 and Gd_2O_2S has increased notably in the biomedical field [2,3]. This is due to the excellent optical response of both compounds that can be syntonized in a wide spectral range, from high energy photons (X-ray) to radiation considered transparent to the biological window (750–950 nm) [4]. Moreover, the Gd_2O_3 and Gd_2O_2S have excellent physicochemical properties related to their high optical response, high thermal and chemical stability, and their capacity to be produced in different shapes, particle sizes, and textures. These attributes make them superior compared to other particles [5]. These are important features in the biomedical field since they allow us to have particles with a large surface area that can be functionalized with ligands to target specific biomolecules [6]. However, their production in the micro or nanoscale is a constant challenge. Therefore, numerous synthesis and functionalization strategies have been approached to enhance both systems' intrinsic properties in recent years. The synthesis methods for their preparation include techniques such as sonic-chemical reaction [7], solid-state reaction [8], the sol-gel method [9], polyol method [10], microwave-assisted synthesis [11], the hydrothermal method [12], and combustion synthesis method [13]. These

techniques are widely used to produce well-shaped nano- or micro-particles doped with different ions. However, differences in the quantum efficiency or optical responses among the reports have also been observed [1,3,14]. Moreover, these synthesis routes also produce samples with low crystallinity, defects on the particle surface, and the generation of organic by-products that are difficult to remove and limit their application in the biological field [15].

On the other hand, recently, a variety of novel biomedical applications for Gd_2O_3 and Gd_2O_2S have been discovered, which include their use as antimicrobial agents [16], transport vehicles [17], therapeutic agents [18], and nanovaccines [19]. These applications have emerged because of particle surface functionalization and by obtaining particles with specific sizes and shapes. However, the appropriate selection of Gd_2O_3 or Gd_2O_2S for use in these applications is not yet clear. However, recent reports reveal that Gd_2O_2S is more promising due to its superior quantum efficiency than Gd_2O_3 [20]. In this regard, our work presents a compilation of the recent studies of gadolinium-based oxides and oxysulfides to establish a critical analysis and prospects for their use in the biomedical field. To this end, we have reviewed the different synthesis methods and various functionalization strategies that have allowed their novel applications.

2. Optical Properties of Gadolinium-Based Oxide and Oxysulfide Materials

2.1. Gadolinium-Based Oxide

Rare-earth oxides are advanced materials widely used as host lattices to develop sensors and luminescent materials [21]. They are recognized for their excellent chemical and thermal stability [22], low phonon energy (~300–600 cm^{-1}), and the facility on which they can be doped with lanthanide ions [23,24]. Gadolinium oxide (Gd_2O_3) is considered one of the most promising materials for developing contrast agents for magnetic resonance and fluorescence imaging [25]. This is due to the trivalent state of gadolinium inside the matrix that induces a highly stable 4f shell with seven unpaired spins, making it strongly paramagnetic [26]. Likewise, the intrinsic optical properties of Gd_2O_3 render them the ability to producing sharp wavelength absorptions and photostability, which make them useful for imaging applications. The optical properties of Gd-based materials can be enhanced by doping the matrix with other lanthanide ions. Thus, a good selection of doping-ions makes it possible to obtain photoluminescent materials with high Stokes shifts, sharp emission spectra (in the visible or NIR regions), long lifetimes, minimized photobleaching, and multiphoton absorption [27]. Besides, the tuning of the excitation and emission wavelength, as desired. Because of these properties, gadolinium-oxide lattices are considered excellent materials for photoluminescence applications, including not only the technological approach but the biomedical field as well [28].

2.2. Down- and Up-Conversion Emission Processes

Lanthanide ions share a similar electronic configuration, but unlike gadolinium, most of them can exhibit luminescence due to intraconfigurational 4f-4f transitions when excited with UV-Vis or NIR wavelengths [29]. The crystal field might alter lanthanide ions' electronic structure to access this impressive phenomenon [30]. Therefore, to achieve photoluminescence through downconversion (DC) or upconversion (UC) processes, lanthanide ions are placed in minimum quantities into the gadolinium host lattices.

The most common process to obtain a photoluminescence emission is by DC [31]. In this process, high-energy photons are used to excite electrons from their ground state to a higher energy level inside the host lattice. After that, the energy is transferred to a luminescent ion, and the energy dissipates by radiative relaxation (a luminescent emission occurs) [32]. In this case, the host lattice's gadolinium acts as a sensitizer (which absorbs the excitation energy), and the other lanthanide ions act as an activator (which usually releases radiative energy).

On the other hand, the UC phenomenon occurs when low-energy photon absorption is transformed into a high-energy photon emission [33]. Three mechanisms can explain this

phenomenon: (1) the energy transfer (UC-ETU), (2) the cross-relaxation (UC-CR), and (3) the energy state absorption (UC-ESA). A schematic representation of each mechanism is shown in Figure 1. The UC-ETU is the most common path to obtain UC photoluminescence [34]. In this process, both the sensitizer and activator must be in the crystal lattice as doping ions. The sensitizer should be selected for its multiphoton absorption capacity of NIR wavelengths, and the activator must have coupled energy levels with the sensitizer's excited state [35,36]. Two or more photons absorbed by the sensitizer can create a virtual energy level paired with the activator's energy level during the absorption process. Then, the sensitizer transfers the absorbed energy to the activator, making a radiative relaxation to the ground state (see Figure 1).
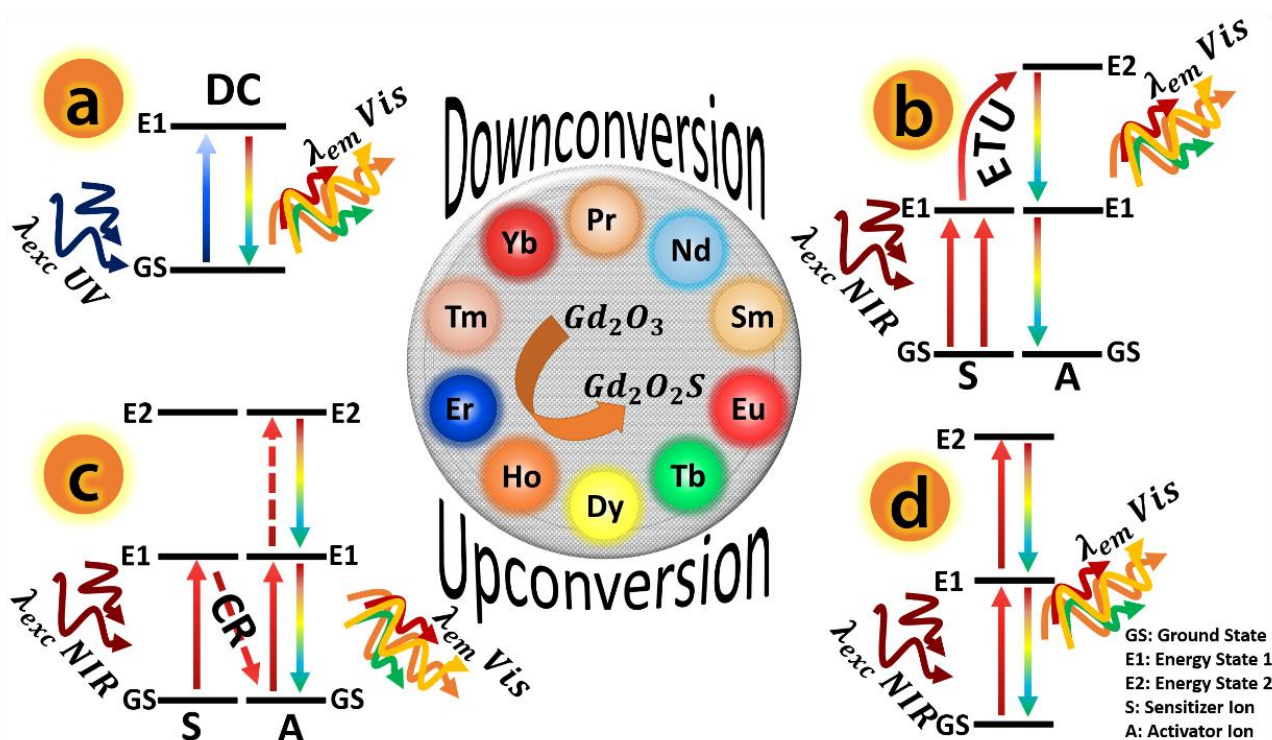
Figure 1. Lanthanide photoluminescence phenomena achieved in gadolinium oxide and oxysulfide materials. The most common mechanisms that involve photoluminescence include the following: (**a**) downconversion (DC), (**b**) energy transfer upconversion (UC-ETU), (**c**) cross-relaxation (UC-CR), (**d**) energy state absorption (UC-ESA) graphically explained in energy level diagrams.

The UC-CR takes place when several energy levels exist with a similar energy gap. Most of the time, the cross-relaxation is undesired for the luminescence because it decreases the emission intensity by phonons; however, it can be managed to obtain luminescent emission under specific excitation conditions. This process is achieved by using a sensitizer and an activator. Both must have two or more energy levels with a similar energy gap. After the sensitizer has absorbed the excitation energy, some relaxation transitions release energy, which is used to excite certain energy levels of the activator, resulting in multiple excitations within the activator and high energy emission wavelengths [37].

The energy state absorption (UC-ESA) can be accomplished by using lanthanide ions with a ladder-like energy level configuration. In this process, the same ion can act as a sensitizer and activator. Because of the ladder-like arrangement, an absorbed photon after NIR excitation can promote an electron to the first excited state. Still, a successive second absorption can excite the same electron to a higher energy level, from which a radiative transition to the ground state occurs [13].

Due to these mechanisms, the lanthanide-doped gadolinium oxides and sulfides can virtually absorb the whole electromagnetic spectrum from UV to NIR. Moreover, the energy

can be transformed into visible luminescence, which is very attractive for contrast, imaging, and sensing applications [38].

2.3. Dopants and Their Effect on the Photoluminescence Emission of Gd2O3

Gadolinium-based oxide and oxysulfide host lattices are highly compatible with other lanthanide ions. Therefore, photoluminescence can be tuned with the desired color emission under a required wavelength excitation through their appropriate selection. Over the past ten years, different photoluminescent materials based on lanthanide-doped gadolinium oxide have been widely studied. Figure 2a–c depict the analysis of a careful search of Gd_2O_3 materials doped with varying lanthanide ions. For this analysis, 131 published studies were collected from Google Scholar© under the search "gadolinium oxide photoluminescent materials" and "Gd_2O_3 doped photoluminescent materials".

Figure 2. General features of photoluminescent processes by downconversion and upconversion in gadolinium oxide lattices. (**a**) Percentage of publications in the last ten years on the design of gadolinium-based matrices for upconversion or downconversion phenomena. (**b**,**c**) The most widely used lanthanide dopant. (**d**) Excitation and emission spectra of Eu-doped gadolinium matrices. (**e**) Excitation and emission spectra of Tb-doped gadolinium matrices. (**f**) Energy level diagram and luminescent emission processes in Eu-doped gadolinium matrices. (**g**) Emission lines of Er, Tm, and Ho were used as dopants in Gadolinium matrices. (**h**) Photograph of the photoluminescent emission by upconversion of Gd-based particles with different dopants in colloidal suspension. (**i**) Energy levels diagram describing the radiative and non-radiative processes in Gd-based lattices by upconversion using Yb, Er, and Tm as dopants.

Europium (Eu) is the most common activator ion used to study and recognize the photoluminescence in gadolinium lattices (see Figure 2b). Figure 2d shows the excitation and emission spectra of an Eu-doped gadolinium oxides material. After a 255 nm excitation, an intense red color can usually be detected even by the naked eye [39]. The red color is attributed to the $^5D_0{\rightarrow}^7F_2$ transition, which appears at ~613 nm, as shown in the energy level diagram of Figure 2f. The UV radiation (~250 nm) absorbed by the gadolinium from the host lattice promotes the electrons from its ground state to the ^5L_J energy levels

of the europium ion, from which several non-radiative transitions occur up to the $^5D_0$ energy level, finally the characteristic radiative transitions $^5D_0{\rightarrow}^7F_J$ take place. Terbium (Tb), on the other hand, gives a bright green color luminescence after UV excitation of the gadolinium lattices [40]. As it can be seen in Figure 2e, this color corresponds to the transition $^5D_4{\rightarrow}^7F_5$ which lies in 545 nm. The color can be noted in the inset of Figure 2e.

Regarding the upconversion (UC) luminescence, the most used lanthanide ions are depicted in Figure 2c, with ~40% frequency for both Ytterbium (Yb) and Erbium (Er), which are the most used doping ions to obtain UC. Yb is an excellent sensitizer for NIR radiation. After being excited at 980 nm, Yb can efficiently transfer the harvested energy to Er [41], Tm [42], Ho [43], or other lanthanides, and the photoluminescence can be detected, as shown in Figure 2g. The characteristic colors obtained under NIR radiation can be observed in Figure 2h, which shows how the upconversion luminescence can be tuned depending on the activator ion used. The versatility of Yb to be paired with other activator ions makes it possible to obtain gadolinium-based lattices with different color emissions. This versatility can be explained by the energy level diagram in Figure 2i, where Yb is the sensitizer that, after multiple photon absorption, can transfer its energy (UC-ETU) to several energy levels of the paired activator ions whose radiative transitions lay in different sections of the visible spectrum. Following this outcome, the Yb/Er combination is the most common to obtain a successful gadolinium oxide upconverting material. However, using Yb as a sensitizer makes it possible to bring other luminescent colors upon 980 nm excitation [44].

2.4. Dopants and Their Effect on the Photoluminescence of Gd_2O_2S

Another advantage of gadolinium oxide material is the possibility of obtaining gadolinium oxysulfide phosphors by using them as precursors in a solid-state sulfidation reaction [45]. Gadolinium oxysulfide shares some properties with its precursors, such as high thermal and chemical stability, insolubility in water, and high absorption of light [46]. However, some properties are enhanced with respect to other materials. Gadolinium oxysulfides are better luminescent materials than their precursor oxides or sulfides and exhibit high quantum yield efficiency compared with fluorides [47]. These properties make oxysulfides promising materials in the bioimaging field [48,49]. The luminescent mechanisms are not affected despite the host lattice used to contain the selected lanthanide ions.

Gadolinium oxysulfides, on the other hand, are less studied than oxides. In the last ten years, only 27% of the 179 retrieved publications referred to lanthanide-doped gadolinium oxides, and oxysulfides belonged to studies related to oxysulfide luminescent materials (see Figure 3). The main reason is the complicated processes required to obtain oxysulfide materials [50,51] that might compromise the precursors' initial morphology, affecting the materials' luminescence properties [25]. Nonetheless, novel strategies are being explored nowadays to avoid the stringent processes to obtain oxysulfides without compromising the optical properties. Another issue is the frequent requirement of toxic precursors; thus, the synthesis should proceed in environmentally controlled conditions.

In Figure 4, some relevant examples of gadolinium oxysulfide materials used as a host lattice for luminescent phosphors are depicted. The synthesis of oxysulfide materials mainly focuses on three luminescent phenomena, as shown in Figure 4a, where the radioluminescence is an alternative application of oxysulfides apart from DC and UC. DC is still the most studied process upon lanthanide-doped oxysulfides, highlighting europium and terbium as the most utilized lanthanide dopants to obtain photoluminescence (see Figure 4b). The europium-doped gadolinium oxysulfide excitation-emission spectra are depicted in Figure 4d. Although the emission color corresponding to the transition $^5D_0{\rightarrow}^7F_2$ is the same as in the oxide, there is an important difference in the emission spectrum structure. In the europium-doped oxide material, the $^5D_0{\rightarrow}^7F_2$ transition has a maximum peak at 613 nm, whereas in the oxysulfide, the maximum peak is located at 623 nm. This difference is due to the crystal field environment and provides information about the

doping ions' position in the host lattice [50]. Despite this difference, europium-doped oxysulfide materials are recognized as red phosphors applied in technological applications.
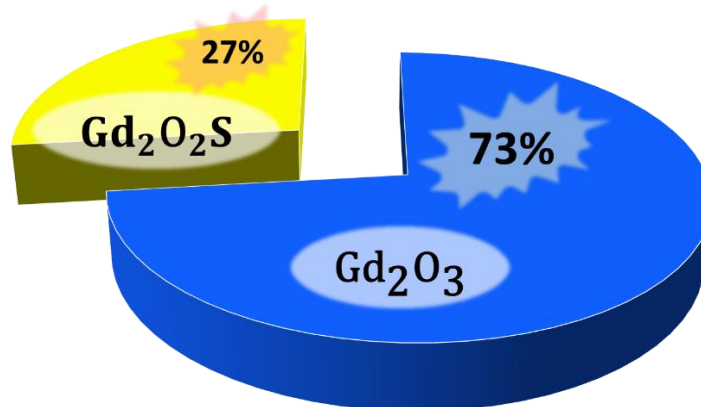
Figure 3. State of the art for gadolinium-based oxide and oxysulfide luminescent materials. Comparison of the preferential research between oxides and oxysulfides over a total of 179 publications from the last ten years.
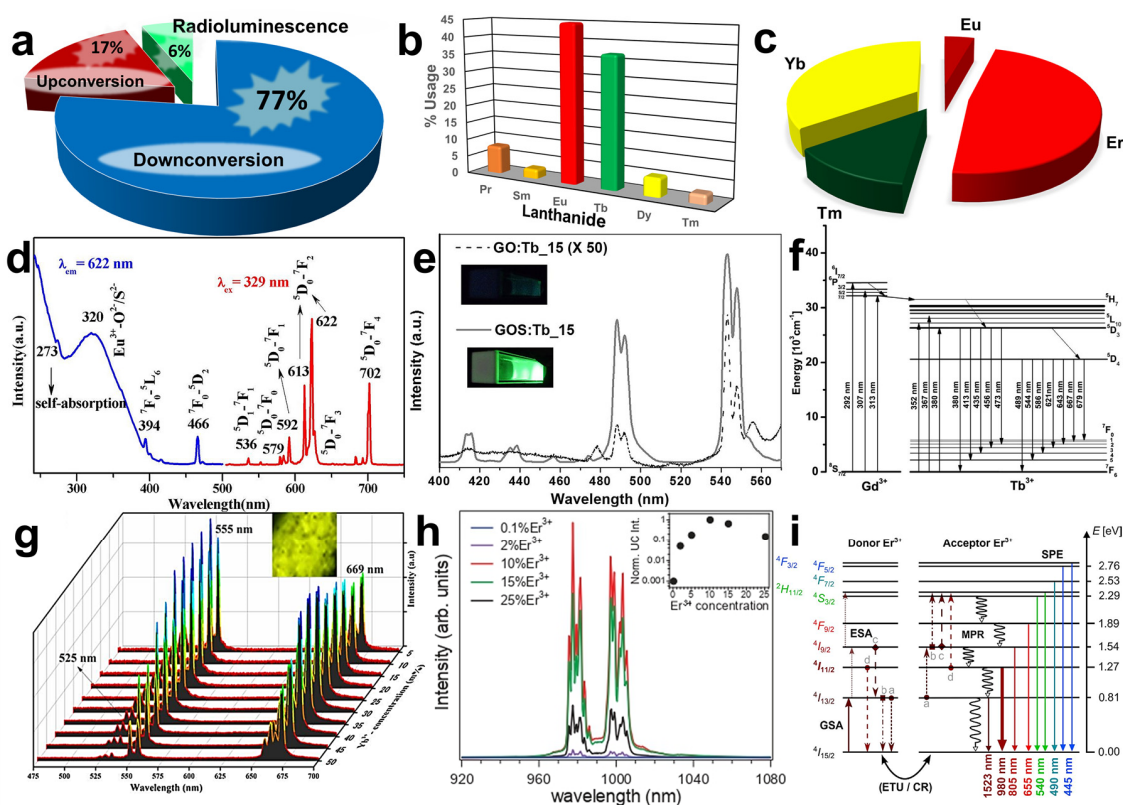
Figure 4. Gadolinium oxysulfide materials and their general applications: (**a**) main applications of gadolinium oxysulfides in the last ten years, (**b**) lanthanides employed as dopants to achieve downconversion processes, (**c**) most employed lanthanide dopants for gadolinium oxysulfide upconversion materials, (**d**) fluorescence excitation/emission spectra of a Gd_2O_2S:Eu material where the principal excitation-emission is detected at 622 nm, (**e**) fluorescence emission spectrum of a Gd_2O_2S:Tb material and (**f**) the corresponding energy level diagram representing the main transitions that make possible the green coloration at room temperature, (**g**)visible upconversion emission of a Gd_2O_2S:Yb/Er material under different Yb concentrations, the excitation energy employed was 980 nm at room temperature, (**h**) upconversion luminescence spectra of gadolinium oxysulfide materials with different concentrations of Er upon excitation at 1510 nm and (**i**) energy level diagram of a Gd_2O_2S:Er material showing all the processes involved in the luminescence phenomena.

Another recognized phosphor is the terbium-doped oxysulfide, which is characterized by its bright green color often used in radioluminescence applications [14,51]. Figure 4e shows the photoluminescence emission spectra of terbium doped oxide and oxysulfide materials, where the intensity of oxysulfides is up to fifteen times greater than its oxide precursor. This study has highlighted the importance of more research related to photoluminescent oxysulfides. Moreover, the downconversion mechanism is depicted in Figure 4f. The host lattice absorbs the UV radiation (~290 nm) and is transferred to the terbium ions that release the energy in several radiative transitions resulting in a visible green color.

Although studied in a minor proportion, upconverting gadolinium oxysulfides are exciting and valuable materials. The most used lanthanides to achieve this phenomenon are depicted in Figure 4c. It can be seen that Yb and Er are still the most used ions to develop upconverting materials. Figure 4g shows a set of experiments carried out to find the optimum Yb/Er composition. The luminescence of the materials is depicted in the inset. A green-yellowish coloration is observed after irradiation with a 980 nm diode laser. The UC-ETU is the mechanism that explains this coloration, as described before.

Figure 4h shows another approach. In a series of experiments where only Er is used as the dopant ion, the optimum concentration to obtain the most intense luminescence was 10%. The UC-ESA was the primary mechanism leading these results, which is explained in Figure 4i. Erbium ion possesses a ladder-like energy level structure that can promote electrons to higher energy levels in the UV region after multiple photon absorption. As it can be observed in the picture, after successive absorption of 980 nm or 1150 nm excitation energy, the $^4I_{13/3}$ energy level is reached, from which the electrons are promoted to $^4I_{9/2}$, and $^4S_{3/2,}$ energy levels. A further energy transfer between erbium ions can lead to high energy emissions in the blue color (~450 nm).

Additionally, cross-relaxation processes can occur (labeled in a–d), which leads to exciting $^4S_{3/2}$ energy levels. The radiative transitions to the ground state give the characteristic green coloration (~540 nm). Finally, the red color is attributed to the $^4F_{9/2} \rightarrow {}^4I_{15/2}$ transition, which is a consequence of cross-relaxation processes followed by some non-radiative transitions from $^4S_{3/2}$ to $^4F_{9/2}$.

For the case of oxysulfides, erbium is mainly used as a sensitizer comparing with ytterbium. There is no specific reason for this trend. Erbium has the same versatility as ytterbium, with the difference that erbium can absorb different wavelengths in the NIR infrared spectrum, while ytterbium is limited only to 980 nm energy absorption.

3. Status on Gadolinium-Based Nanoparticles Synthesis

3.1. Gd₂O₃ Synthesis Routes

Several routes to synthesize gadolinium-based oxides have been reported. A summary of the most used synthetic routes is depicted in Figure 5. These pathways include the wet chemical route, solid-state process, bioreduction process, "polyol" protocol, reverse phase microemulsion, sonic chemical method, combustion method, precipitation method, and hydro/solvothermal method. Some of the newest strategies that have been developed are described below.

3.1.1. Sonic-Chemical Method

Perdigon-Lagunes et al. [7] reported the synthesis of β-Gd and Gd₂O₃ NPs via the sonic-chemical method at room temperature through an alkaline reduction synthesis using tannic acid as a reductive agent. In their report, a Gd(NO₃)₂ solution and tannic acid were mixed. An appropriate amount of NaOH was added under stirring to regulate the pH to different values (5, 8, 9, and 11). The resulting dissolution was sonicated for 5 min to activate all clustering sites. Gd³⁺ was reduced to Gd(0) atom, which binds with other Gd(0) into metallic clusters. The formed clusters serve as seeds of nano particles. This method used a cavitation process produced by the addition of highly localized energy from ultrasonication. The nanoparticle clusters were oxidized by the oxygen present in the aqueous solution. The nanoparticle growth was limited by freezing the reaction mixture

in liquid nitrogen. The lyophilization process then removed the solvent. The size and structure of formed NPs were pH-dependent due to the pK_a of tannic acid. Overall, the dimensions of the NPS synthesized under different pHs media were below 7 nm.
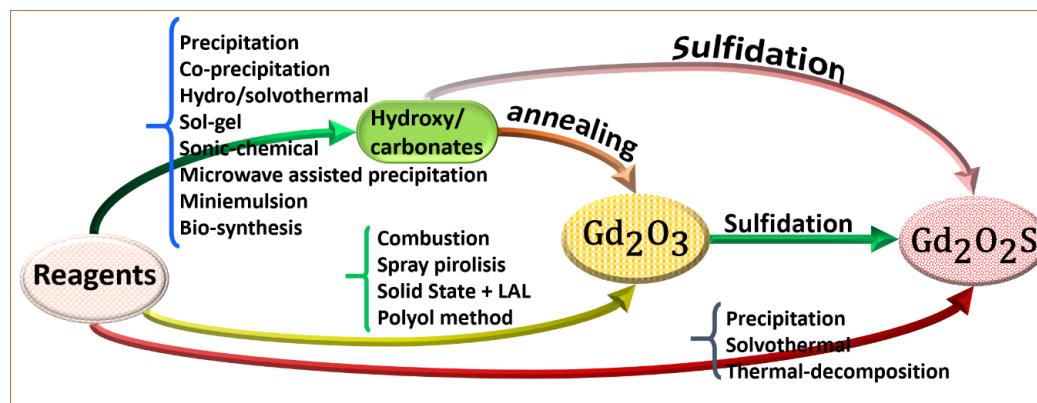
Figure 5. Synthesis routes to produce gadolinium oxides and/or oxysulfide materials at the micro and nano level.

3.1.2. Solid-State Technic

Chen et al. [8] reported the synthesis of Terbium-doped gadolinium oxide nanoparticles (Gd_2O_3:Tb) by the standard solid-state technic combined with laser ablation in liquid (LAL) method. This method's main advantages are; (1) the absence of a reducing agent, (2) the size control of the particles through laser-induced size reduction, the choice of solution or laser parameters. The standard solid-state technic consisted of Gd_2O_3 and Tb_4O_7 milled (in different stoichiometric ratios: 0.5%, 1%, 5%, 10%, and 20% of Tb). Following the LAL method, the obtained solid targets were ablated in liquid by a microsecond laser, with the Gd_2O_3:Tb target fixed on the bottom of a container filled with deionized water. The obtained NPs possess a monoclinic structure without any metallic erbium or terbium oxide phases. XRD patterns analysis suggested a good crystallinity and high purity. Meanwhile, TEM micrographs revealed spherical shapes with an average size of 8.4 ± 0.2 nm. NPs showed an efficient fluorescence due to the extrinsic dopant (Tb ion) and the high r1 value resulting from the Gd_2O_3 matrix host. The Gd_2O_3:Tb (1% mol of Tb) ion was capable of optical labeling, efficient for MR imaging, and did not cause significant cytotoxic effects. These results suggested that Tb-doped Gd_2O_3 is a promising dual-modal contrast agent candidate for fluorescence and MR imaging.

3.1.3. The Sol-Gel Method

The sol-gel method is a wet-chemical technique that involves several steps: (1) hydrolysis and polycondensation, (2) gelation, (3) aging drying, (4) densification, and (5) crystallization. Niftaliev et al. [9] reported gadolinium oxide NPs synthesized by the sol-gel method using $Gd(NO_3)_3$ as the salt precursor and agar-agar as a stabilizer. White gel with a particle size of 145 ± 10 nm was obtained. The gel was frozen in a freezing camera at $-20\,°C$ (this temperature was found to be optimal after different studies) and dried at $100\,°C$ to remove the water from $Gd(OH)_3$ gel. The gel's annealing at $700\,°C$ produced the Gd_2O_3 particles, mainly rounded with an average size of 8–16 nm.

3.1.4. Polyol Protocol

In a recent work published by Ahmad et al. [10], the authors reported the synthesis of ultra-small Gd_2O_3 nanoparticles coated with poly(methyl vinyl ether-alt-maleic acid) (PMVEMA) polymer. The Gd_2O_3 NPs were prepared by the one-pot polyol method. This synthesis method is based on direct rare-earth oxide precipitation in high boiling alcohol. The average diameter size of the obtained particles was 1.9 nm. The ultra-small

size of the particles is appropriate because they are more easily renal excreted, make them ideal for in vivo applications. The two carboxylic acid functional groups present in PMVEMA produced a strong interaction among the polymer and Gd_2O_3 NPs through multiple coordination bonds. This created an enhancement in the colloidal stability and the relaxometry properties (r_1 = 36.2 s^{-1} mM^{-1}, and r_2 = 74.0 s^{-1} mM^{-1}) in which the r_1 value was approximately 10 times greater than those of commercial molecular contrast agents. Besides, the PMVEMA is a hydrophilic and biodegradable biopolymer making the Gd_2O_3 NPs biocompatible. The PMVEMA-coated ultra-small Gd_2O_3 NPs exhibited high positive contrasts in vivo T_1 MR images after intravenous administration, demonstrating their effectiveness as a T_1 MRI contrast agent.

Guleria, A. et al. [52] reported the effect of polyol chain length on size and proton relaxivity of Gd_2O_3 NPs for enhanced magnetic resonance imaging contrast. The authors studied the influence of various polyols with different reductive abilities on the size and morphology of prepared Gd_2O_3 surface-coated NPs. The studied glycols were diethylene glycol (DEG), triethylene glycol (TEG), tetraethylene glycol (TeEG), and polyethylene glycol (PEG 2000). They observed that the size of the obtained NPs is dependent on the chain glycol length, which means particle size increase with the increase of chain length. TEM analysis revealed that all the Gd_2O_3 nanosystems consist of spherical nanoparticles and their agglomerates. The rise in polyol chain length significantly increased in vitro and ex vivo r_1 and r_2 proton relaxivities. PEG-Gd_2O_3 exhibits the highest in vitro r_1 and r_2 values of 5.75 and 28.7 $mM^{-1}s^{-1}$, respectively.

3.1.5. Hydrothermal Method

The hydrothermal synthesis consists of the precipitation of gadolinium hydroxides under high temperature and pressure [53]. This methodology is highly recommended for the synthesis of anisotropic structures. Nanorods and nanowires are the most often low dimensional nanostructures synthesized by this methodology, although spherical nanoparticles can be obtained under these conditions [19].

In a typical synthesis, the lanthanide precursors solution is mixed with the precipitation agent, which in this case can be ammonia [54], KOH [55], NaOH [56], or urea [57]. After several minutes of stirring, the mixture is placed into a Teflon-lined autoclave, sealed, and heated to the reaction conditions. The hydrothermal synthesis is characterized by its high reaction temperatures above 150 °C and long reaction times, from 6 to 24 h. However, it offers good homogeneity, reproducibility, and high purity of the obtained hydroxide products [58].

Sometimes the water used as a solvent media is replaced for glycol [59], toluene [60], oleylamine [61], or other organic solvents, then the synthesis is referred to as solvothermal. Precipitation agents, on the other hand, are not limited to hydroxides since ethanolamine [19], triethylamine [62], or peroxides [63] are also used in the synthesis of anisotropic nano/microstructures.

Chaudhary S. et al. [64] reported the synthesis and characterization of Gd_2O_3 NPs functionalized with ethylene glycol (EG) by the hydrothermal method starting from $GdCl_3$ and EG. A variation on $GdCl_3$ concentration was done from 5 mM to 25 mM to study the effects of synthetic parameters over the optical, photoluminescence, and band-gap variation. The nanoparticles have shown crystallites with an irregular pseudo-spherical shape and a size distribution between 7–15 nm. The nanoparticles were tested as proficient electrocatalytic material to detect hydrazine and p-nitrophenol using neutral pH cyclic voltammetric and amperometric methods. The developed sensor exhibited a linear range of 1 to 10 μM with a low detection limit of 1.527 and 0.704 μM for p-nitrophenol and hydrazine. The sensitivity, selectivity, repeatability, recyclability, wide linear range, and detection limit make Gd_2O_3 NPs a favorable nanomaterial for detecting pollutants.

Wu et al. [65] reported synthesizing hyaluronic acid-functionalized Gd_2O_3 NPs (HA-Gd_2O_3 NPs) by a one-pot hydrothermal approach. Prepared NPs showed an average diameter of 105 nm exhibiting uniform dispersion and quasi-spherical shape. The incor-

poration of HA confers the Gd_2O_3 a favorable water dispersibility, low cytotoxicity, and excellent biocompatibility. Bifunctional HA-Gd_2O_3 NPs presented a promising potential for tumor diagnosis and radiotherapy.

3.1.6. Microwave-Assisted Gd_2O_3 NPs Synthesis

Trinh et al. [11] reported the rapid synthesis of TEG-coated Gd_2O_3 NPs by a modified polyol method with microwave assistance using TEG (triethylen glycol) solvent and surfactant stabilizing agent. TEG-coated Gd_2O_3 NPs sizes could be controlled by changing synthetic parameters such as $GdCl_3$ concentration, reaction time, and reaction temperature. After thermal treatment formed Gd_2O_3 NPs showed spherical shapes. The obtained particle sizes were 1 nm, 5 nm, and 10 nm.

Surendra et al. [66] reported the synthesis of Gd_2O_3 NPs by green synthesis process using the methanolic extract of Moringa oleifera (M. oleifera) peel. The synthesis was performed by microwave-irradiation method mixing $Gd(NO_3)_3$ and extract of M. oleifera, the mixture was then irradiated at 300 W in a microwave (MW) system. After purification, Gd_2O_3 NPs were calcinated at 300 °C. The synthesis was optimized by response surface methodology (RSM) joint with Box-Behnken (BBD) design. The bioreduction mechanism consists of the presence of different molecules in M. oleifera peel such as phenols, terpenoids, and flavonoids that act as reductive agents; dissolution of $Gd(NO_3)_3$ $5H_2O$ dissociates Gd^{3+} and NO^{3-}. Gd^{3+} ions are attracted by the M. oleifera extract, converting Gd^{3+} into Gd^{2+}. Bioreduction results in the formation of Gd_2O_3 NPs. Prepared NPs presented rod shape and 26 ± 2 nm size. The NPs showed moderate antifungal activity against Alternaria saloni and Sclerrotium rolfsii and good antibacterial activity against Gram (+) and Gram (−) bacteria.

Vahdatkhah et al. [67] reported synthesizing coated polyvinyl pyrrolidone (PVP) ultrasmall Gd_2O_3 NPs by a microwave-assisted polyol technique. NPs were synthesized below five minutes. $Gd(NO_3)_3$ $6H_2O$ was dissolved in diethylene glycol (DEG) and heated at 100 °C overnight. NaOH was then added, and the reaction mixture was microwave irradiated under an O_2 atmosphere. The reaction mechanism involved two steps: (1) metal ion complexation and (2) hydrolysis/condensation. In the first step, alcohol groups from ethylene glycol (EG) were oxidized in the presence of nitrate ions to the aldehyde and then to diglycolic acid. In the second step, NaOH was used as a hydrolysis agent. Substitution of hydroxyl groups in nitrate ions formed gadolinium hydroxide ($Gd(OH)_3$). Dehydration of $Gd(OH)_3$ through microwave irradiation produced Gd_2O_3. Afterward, surface modification of Gd_2O_3 with PVP was performed, obtaining spherical-shape-coated NPs of 2.5 ± 0.5 nm size.

3.1.7. The Mini Emulsion Technic

Zhang et al. [68] reported synthesizing spherical Ln-containing nanoparticles (Ln = Gd, Ho) by a novel microemulsion method. This method allowed reasonable control of NPs size in the 5 to 40 nm range. The synthetic methodology involved two steps: (1) Ln nanodroplets' were prepared by mixing lanthanide acetylacetonate ($Ln(acac)_3$) with $CHCl_3$ or DCM. The mixture was added dropwise to a continuous phase consisting of Brij® 35, a nonionic polyoxyethylene surfactant to get Ln_2O_3 NPs or sodium dodecyl sulfate (SDS) to get $Ln_2O_2SO_4$ NPs. Obtained suspensions were ultrasonicated, yielding a microemulsion. (2) Hydrophobic solvents were removed and then freeze-dried yielding Ln containing powders. (3) The previously obtained powders were thermally decomposed by calcination at 800 °C under aerobic conditions.

3.1.8. Biosynthesis

Khan et al. [69] reported for the first time the extracellular biosynthesis of protein capped Gd_2O_3 NPs by using thermophilic fungus *Humicola* sp. Synthesized nanoparticles were bioconjugated with the chemically modified anticancer drug taxol (2′-glutarylhexanediamine taxol). The synthesis of Gd_2O_3 NPs was performed by mixing $GdCl_3$ and the harvested

mycelial mass of fungus *Humicola* sp at basic pH and heated at 50 °C in the dark. Bio-conjugation of chemically modified taxol was carried out by the covalent bond formation between the capping protein carboxylic acid group and the 2′-glutarylhexanediamine taxol amino groups.

3.1.9. Thermal Decomposition

Dedkova et al. [70] reported the synthesis of Gd_2O_3 NPs by the thermal decomposition of the complex formed in situ from $Gd_2(NO_3)_3$ $6H_2O$ and glycine. Obtained particles had an average size of 10 nm in a net-like structure created by the aggregation of nanoparticles. Antibacterial assays showed a promising potential against four human pathogens.

3.1.10. Combustion Method

The combustion method is one of the most used strategies to obtain gadolinium oxides, which offers short reaction times and high purity oxides. It is a simple methodology involving gadolinium and lanthanide salts (usually nitrates or chlorides) and organic fuel (glycine, urea, among others) [71]. In the method, the lanthanide precursor solution is mixed with the fuel for several minutes at room conditions to carry out the reaction. After that, the reaction temperature is raised above 500 °C, leading to the fuel's instantaneous combustion and generating the gadolinium oxide materials. Jayasimhadri et al. [72] synthesized gadolinium oxide nanophosphors by this methodology. They used glycine as organic fuel and the selected oxide reagents (Gd_2O_3 and Dy_2O_3) in a stringent acidic media of HNO_3. The mixture is pre-heated at 500 °C. The reported reaction was described as follows:

$$6\,RE\,(NO_3)_3 + 10\,NH_2CH_2COOH \;\rightarrow\; 3\,RE_2O_3 + 20\,CO_2 + 25\,H_2O + 14\,N_2 \qquad (1)$$

Moreover, to enhance the crystallinity of the products, an annealing treatment was carried out under temperatures above 1000 °C, obtaining highly crystalline nanoparticles in the range of 35 nm. Some other organic compounds used as fuels have been glucose [73], polyethylene glycol [43], and sucrose [74]. The reaction can be conducted in a hot plate or a furnace, depending on the annealing temperatures. Generally, no post-treatment or purification is needed as the organic compound is consumed, and the by-products evaporate due to the high temperatures of the reaction.

3.1.11. Precipitation Method

The precipitation of lanthanide hydroxycarbonates was first proposed by Matijevic et al. [75]. This method is based on the thermal decomposition of urea into carbonate groups in a water solution. The chemical decomposition of urea and formation of lanthanide carbonates was described by D. Li et al. [76] with the reactions 2 to 4 as follows:

$$(NH_2)_2CO + H_2O \;\rightarrow\; 2\,NH_3 + CO_2 \qquad (2)$$

$$NH_3 + H_2O \;\rightarrow\; NH_4^+ + OH^- \qquad (3)$$

$$2\,Gd^{3+} + 6\,OH^- + 2\,CO_2 \;\rightarrow\; Gd_2O(CO_3)_3 \cdot H_2O + 2\,H_2O \qquad (4)$$
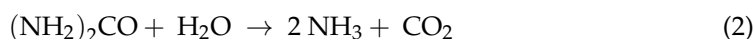
In a typical synthesis, the lanthanide precursors (usually nitrates or chlorides) are diluted in water and stirred for several minutes. Then a urea solution is added to obtain a clear mixture. The precipitation is promoted by heating at 80–90 °C for at least 30 min to get a colloidal mixture of gadolinium carbonates. In this methodology, temperature and stirring are considered critical factors because they regulate the urea degradation rate and delivery of carbonate ions, forming complexes with the Ln ions achieving particle nucleation. Hernández-Adame et al. [77] reported that precursor concentration and reaction time modulate particle size and shape. The authors obtained gadolinium oxide nano-microparticles by controlling the concentration of lanthanide precursors, urea reagent, and reaction temperature. In their work, perfect spherical nanoparticles were prepared by

optimizing the reaction conditions. Moreover, ellipsoidal and seed-like morphologies were obtained in the range of microparticles when the reaction temperature and reaction time were over 100 °C and 40 min, respectively. Several groups have shown that appropriate parameters would produce nano or microparticles with narrow size distribution and exceptional morphological properties. An annealing process obtained the gadolinium oxides. A temperature of 800 to 1100 °C is required to evaporate the carbonates and form the crystal structure of the host lattice. The reaction was reported by Lechevallier et al. [78]

$$Gd_2(CO_3)_3 \cdot 3\,H_2O \xrightarrow{30\ ^\circ C\ <\ T\ <\ 325\ ^\circ C} Gd_2(CO_3)_3 \xrightarrow{325^\circ C\ <\ T\ <\ 530\ ^\circ C} Gd_2O_2CO_3 \xrightarrow{530\ ^\circ C\ <\ T\ <\ 700\ ^\circ C} Gd_2O_3 \qquad (5)$$

This calcination process is carried out after a hydroxide, carbonate, or hydroxycarbonate is formed, and therefore this pathway is recognized as the two-step methodology.

3.2. Gd$_2$O$_2$S Synthesis Routes

It has been reported that Gd_2O_2S production can be carried out by two principal methods: (1) sulfidation process and (2) direct precipitation. Both methodologies are described below.

3.2.1. Sulfidation Process

The sulfidation process of hydroxides or oxides is a treatment required for preparing sulfides or oxysulfides materials. During the first step, the hydroxides or oxides powders are annealed at a high temperature to relax the host lattice, allowing the insertion of sulfur atoms and Gd_2O_2S production [79]. A description of the sulfidation process of gadolinium hydroxycarbonates is depicted in Figure 6. In this procedure, the previously obtained hydroxycarbonates are grounded with sulfur and placed in a cold zone of the furnace. In the beginning, the whole system is degassed using an Ar flow. Then, the precursor sample is moved to a preheated area of the furnace (900 °C) to proceed with the reaction. Due to high temperature, the hydroxycarbonates slowly decompose to oxide compounds, and the sulfur sublimates, flooding the reactor in a gaseous sulfur environment. In these conditions, as the hydroxycarbonate decomposes, it is simultaneously transformed into oxysulfide.

1. Furnace
2. Quartz reactor
3. Gd$_2$O$_3$:Tb sample holder
4. Sulfur powder holder
5. Electrical heating appliance
6. N$_2$
7. Gas flow controller
8. Sulfur gas flow
9. Voltage controller
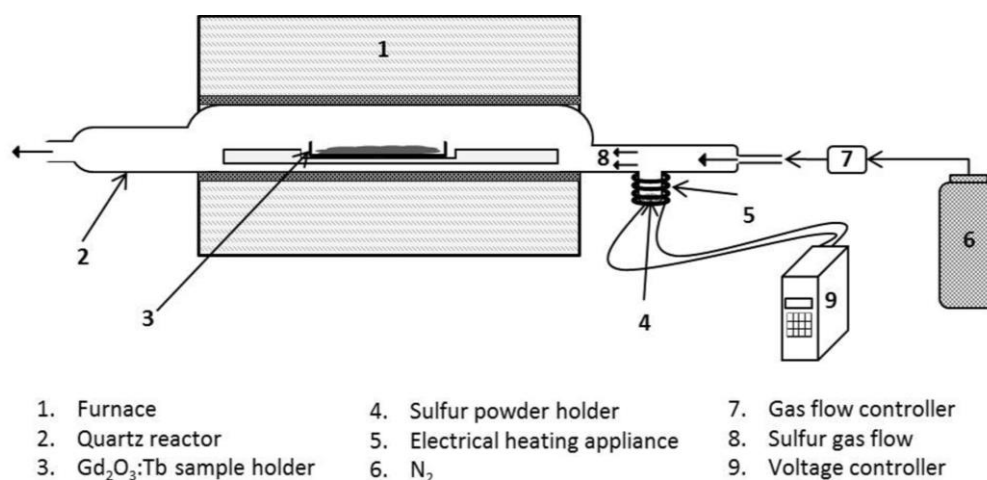
Figure 6. A schematic representation of the sulfidation process consisting of gadolinium-based hydroxides, hydrocarbonates, or oxides exposition to a sulfur atmosphere (image taken with the permission of reference [77]).

The furnace's degassing end is connected to an oil bubbler and a trap with an alkaline solution placed in a fume hood. An environmentally friendly process is achieved with this gas treatment at the furnace outlet (the excess of unreacted sulfur ions is collected in the furnace's cold zone). Some modifications to this system can be seen in the literature. For instance, Hernandez-Adame et al. [77] placed Gd_2O_3 instead of hydroxycarbonates in the

hot furnace zone, the flow of S/N_2 was released through all systems at 900 °C for 2 h to form the Gd_2O_2S single crystals. With these methodologies, high-quality oxysulfides could be obtained without compromising the previously obtained particle size and morphology. Moreover, the synthesis is not limited to a certain quantity of precursors, which can be applied to a large-scale procedure.

3.2.2. Direct Precipitation of Oxysulfides

The aqueous lanthanide solution is mixed with a second solution containing urea and ammonium sulfate in the precipitation method. This latter is considered the sulfur source. The reaction is carried out at 90 °C for 2 h, which are the previously described conditions for the standard precipitation method [80]. After that, purified products were dried and calcined at 800 °C for 1 h to enhance the crystallinity of the freshly prepared microspheres. Lian et al. obtained microspheres using this methodology, which demonstrated the properties of the synthesized oxysulfides and described the chemical reactions involved in this process.

The solvothermal synthesis uses the lanthanide precursors solution and a sulfur source: thioacetamide or ethylenediamine solution containing dissolved sulfur. After stirring, the mixture is placed in an autoclave, and the reaction is carried out at 120–240 °C for 12–24 h. The advantage of this procedure is the direct formation of oxysulfides without needing an annealing process. Thirumalai et al. employed this methodology to synthesize Gd_2O_2S with different shapes and compared the properties of the obtained products with those prepared by the sulfidation process [81]. As a result, the precipitated oxysulfides' chemical surface maintained the organic groups of the selected solvent, which also influenced the crystalline properties of the materials showing an incomplete crystallinity, compared to the bulk oxysulfides obtained by the sulfidation synthesis. However, the solvothermal synthesis offers attractive advantages in the particle shape that can be modulated with the reaction conditions and the solvent selected to precipitate the products.

4. Texture, Shape, and Size of Gadolinium-Based Oxides and Oxysulfides

4.1. Gadolinium-Based Oxides

4.1.1. Porous Gadolinium-Based Sheet-like Particles

Porous nanomaterials have exhibited high drug delivery and release efficacy due to several beneficial properties such as large surface area, surface functionalities, and tunable composition. Recently, Luo et al. [82] reported synthesizing porous Gd_2O_3 nanosheets (Gd_2O_3 NSs) through a two-step colloidal synthesis method. This is the first report exploring the porous gadolinium oxide nanosheets for medical applications. The first step of synthesis was the thermal decomposition with a surfactant, followed by the acid etching with tri-octyl phosphine oxide (TOPO) to obtain porous Gd_2O_3 NSs. TOPO contains weak acids (alkylpohosphonic acids) that could etch Gd_2O_3 to generate vacancies. The obtained Gd_2O_3 NSs exhibited a sheet-like morphology with 142 ± 29 nm in length and an average pore size of 7.53 nm (Figure 7). Gd_2O_3 NSs were later modified by polyetherimide (PEI) and polyethylene glycol (PEG), improving their stability in an aqueous solution. Functionalized Gd_2O_3 NSs showed high doxorubicin (DOX) drug loading capacity. Furthermore, porous Gd_2O_3 NSs showed promising pH-responsive drug release behavior for cancer chemotherapy and can be used for MR imaging applications.
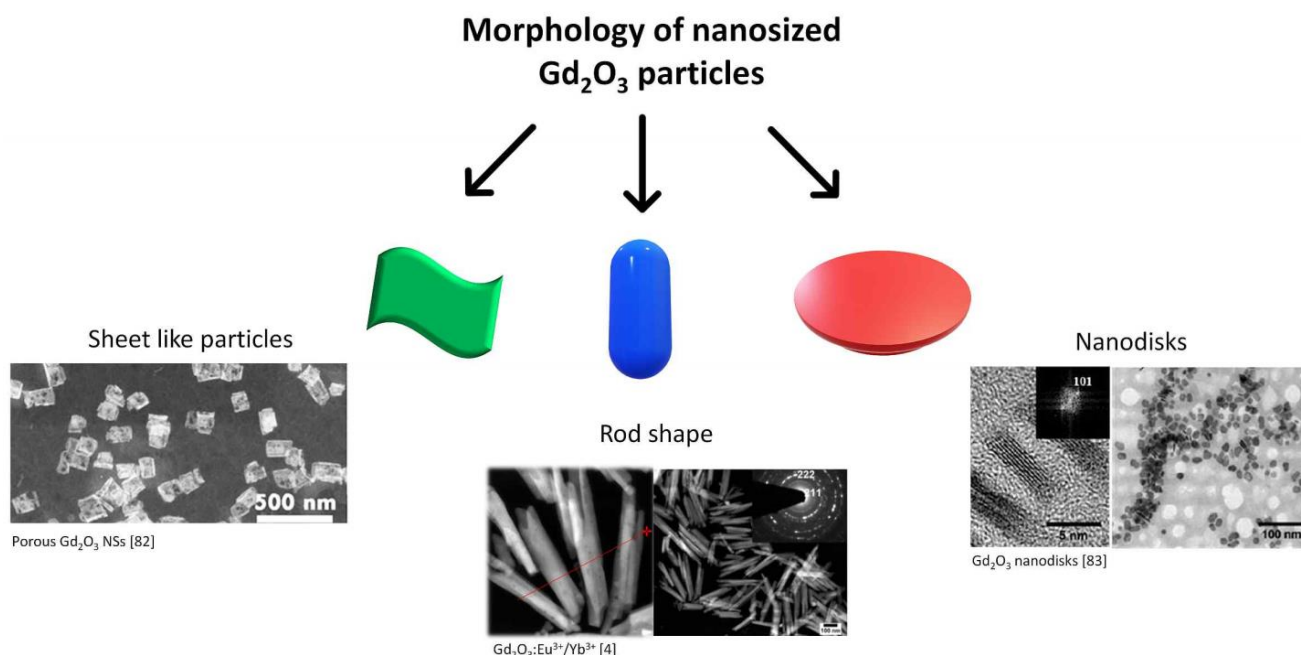
Figure 7. Morphology of gadolinium-based oxides.

4.1.2. Gadolinium-Based Nanodisks

Singh et al. [83] reported synthesizing different sized gadolinium oxide nanodisks through the thermal decomposition of oleate precursor. The Gd-oleate precursor was mixed with oleic acid (OA) and heated at 320 °C under an inert atmosphere. Gd-oleate's thermal decomposition yielded OA capped Gd_2O_3 NPs having a disk shape morphology with a diameter and thickness of 11.2 ± 2 nm and 3 ± 1 nm, respectively (Figure 7). Nanodisks' diameter is OA-concentration-dependent. Higher values of OA produced nanodisks with a larger diameter. The authors tailored the diameter of nanodisks from ~3 nm to ~18 nm. Smaller-sized (>5 nm) nanodisk were suitable to be used as MRI contrast agents.

4.1.3. Gadolinium-Based Spherical NPs

Zhang et al. [68] reported synthesizing spherical Ln-containing nanoparticles (Ln = Gd, Ho) by a novel microemulsion method. This method can control the nanoparticles' size in a 5 to 40 nm range (See Section 3.1.7 for details).

4.1.4. Rod Shaped Gadolinium NPs

Surendra et al. [66] reported the synthesis of Gd_2O_3 NPs by the green synthesis process. Prepared Gd_2O_3 NPs presented rod shape and 26 ± 2 nm size (See Section 3.1.6 for more details).

Del Angel-Olarte reported in 2019 [4] a novel route to produce down and upconverting Eu^{3+}/Yb^{3+} co-doped oxysulfide nanorods, which display solid red emission at 620 nm under Vis (460 nm) or NIR (976 nm) wavelength excitation. The authors performed an in-depth analysis of the synthesis parameters such as lanthanide concentration, type of nucleating agent, reaction temperature, and reaction pressure on the morphology and photoluminescence properties. They demonstrated that as a nucleating agent, ethanolamine is a good substitute for the commonly used triethylamine providing the advantage of using lower toxicity reagents. The nanorods exhibited a 150 nm length and 15 nm diameter (Figure 7).

4.2. Gadolinium-Based Oxysulfides

4.2.1. Spherical Particles

Santelli et al. [84] reported the synthesis of $Gd_2O_2S:Eu^{3+}$ nanoparticles from gadolinium hydroxycarbonates. The first step consisted of an oxidation process at 750 °C for 4 h, followed by solid-gas sulfuration by annealing at 850 °C for 4 h in the presence of sulfur. Electron microscopy of images showed that the $Gd_2O_2S:Ln^{3+}$ have a spherical shape (Figure 8a).
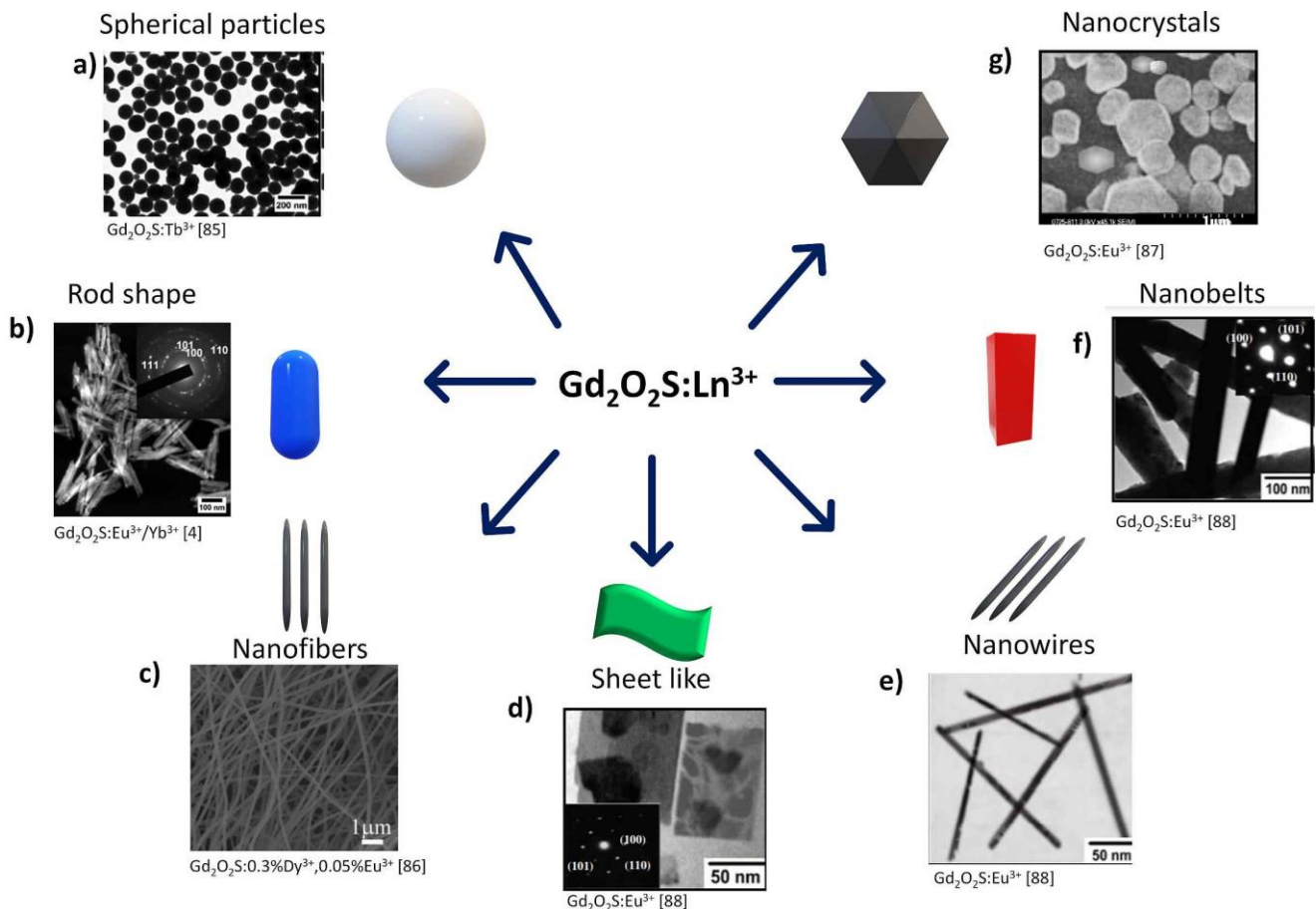
Figure 8. Morphology of gadolinium-based oxysulfide. (**a**) particles with a spherical shape, (**b**) rod-shaped, (**c**) nanofibers, (**d**) sheet-like particles, (**e**) nanowires, (**f**) nanobelts, (**g**) nanocrystals.

Rahim et al. [50] reported synthesizing $Gd_2O_2S:Eu^{3+}$ nanophosphors by microwave irradiation and γ-irradiation methods. FESEM images of obtained particles revealed a spherical nanostructure with diameters of 90 and 50 nm for MW and γ-irradiation synthesis, respectively.

Hernández-Adame et al. [85] reported the synthesis of $Gd_2O_2S:Tb^{3+}$. In this report, the authors studied the influence of the concentration of Tb^{3+} in the luminescence intensity. The dopant concentration ranged from 0.01 to 9% mol. The obtained particles exhibited a spherical shape.

Cichos et al. [79] demonstrated that the morphology of the basic precursors influences the homogeneity and size of Gd_2O_2S (see reference [81] for more details). Shapes of the obtained Gd_2O_2S were mainly spherical.

4.2.2. Submicron Sized Spheres

He et al. [24] reported the synthesis of submicron-sized spheres by a two-step process; (1) amorphous precursor synthesis by the solvothermal method using PVP (poly(vinylpyrrolidone))

as a surfactant to control particle morphology. (2) crystallization to form Gd_2O_2S poly-crystalline spheres using a gas-aided sulfurization process at elevated temperatures. The average particle diameter was observed in the 104–118 nm range.

4.2.3. Nanorods

Del Angel-Olarte reported in 2019 [4] a novel route to produce down and upconverting Eu^{3+}/Yb^{3+} co-doped oxysulfide nanorods, which display solid red emission at 620 nm under Vis (460 nm) or NIR (976 nm) wavelength excitation. The authors performed an in-depth analysis of the synthesis parameters such as lanthanide concentration, type of nucleating agent, reaction temperature, and reaction pressure on the morphology and photoluminescence properties. They demonstrated that as a nucleating agent, ethanolamine is a good substitute for the commonly used triethylamine, providing the advantage of using lower toxicity reagents. The nanorods exhibited a 150 nm length and 15 nm diameter (Figure 8b).

4.2.4. Nanofibers

Chen et al. [86] successfully prepared Dy^{3+}/Eu^{3+} co-doped Gd_2O_2S nanofibers via electrospinning combined with a dual-boat sulfurization approach. Electrospinning is a method to stretch sticky solutions or melts into non-broken fibers or ribbons with a one-dimensional nanostructure. The average diameters of $Gd_2O_2S:0.3\%Dy^{3+}$, $0.05\%Eu^{3+}$ nanofibers were 162.93 ± 0.75 nm (Figure 8c).

4.2.5. Hexagonal Shaped, Nanosheets, Nanobelts, Nanotubes, Nanorods, Nanowires Particles

Thirumalai et al. in 2008 [87] reported a systematic study for the controlled formation of one-dimensional rare-earth-doped oxysulfide nanostructures. The reported synthesis consisted of preparing colloidal rare-earth hydroxides at room temperature and the subsequent hydrothermal treatment at designated temperature and pH conditions. Nanotubes/nanorods can be synthesized by controlling the pH in the solution. The nanotubes/nanorods showed a typical diameter of ~30–50 nm and lengths of up to a few micrometers.

One year later (2009), the same research group reported the hydrothermal synthesis of $Gd_2O_2S:Eu^{3+}$ nanostructures with different shapes [88]. They reported the preparation of single-crystalline $Gd_2O_2S:Eu^{3+}$ with various morphologies: nanocrystals/nanoplates (Figure 8g), nanosheets, nanobelts, nanotubes, nanorods, and nanowires via the hydrothermal process. The authors investigated in detail the influence of experimental conditions such as temperature, reactant ratio, and pH on the final morphologies of products. The synthesis was conducted at room temperature without any additives, catalyst, or template to guide the directional growth of nanosheets (Figure 8d), nanobelts (Figure 8f), nanotubes, nanorods, and nanowires (Figure 8e). Authors found that the driving force for the anisotropic growth of $Gd_2O_2S:Eu^{3+}$ nanostructures derives from the inherent crystal structure of $Gd(OH)_3$ materials and their chemical potential in solution.

5. Surface Chemistry and Functionalization Strategies on Gadolinium-Based Oxides and Oxysulfides
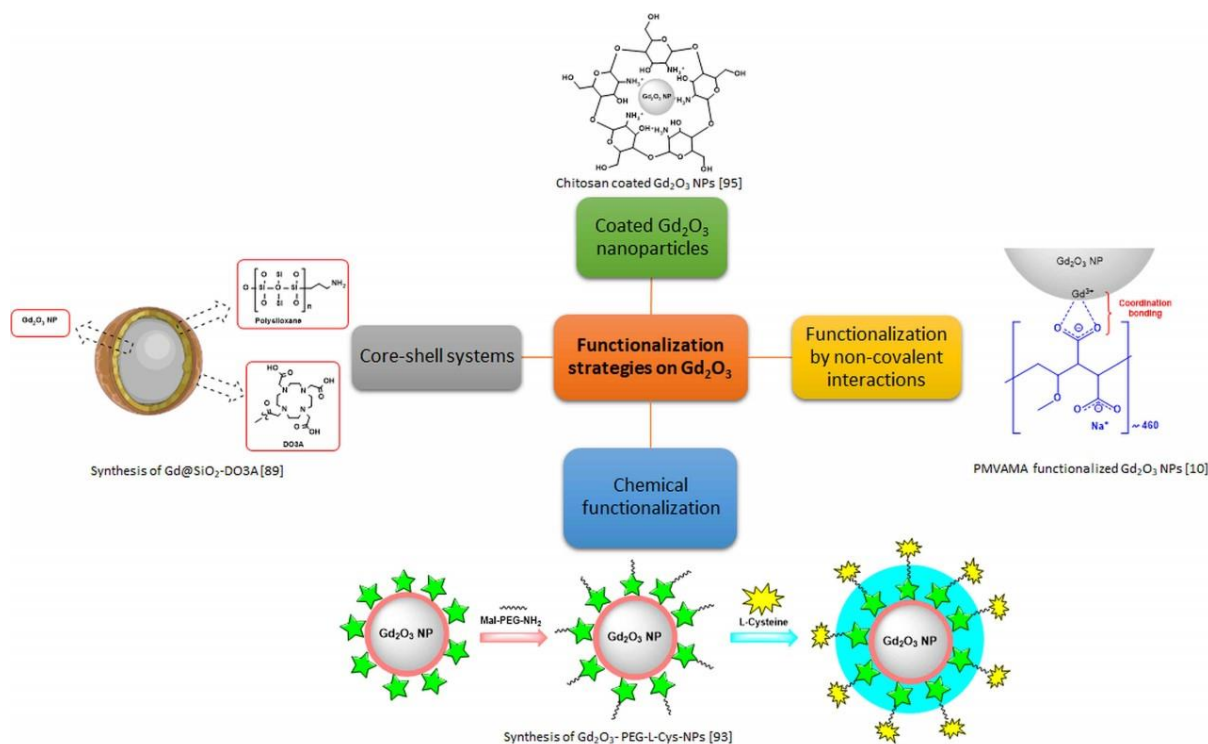
5.1. Gadolinium-Based Oxides

The surface chemistry of gadolinium-based particles can be designed depending on their application. For instance, some organic molecules might be adsorbed on particle surfaces in the biomedical field to achieve the biological target and enhance their biocompatibility, biodistribution, and bioaccumulation properties. Moreover, some reports have shown that surface energy influences the intensity of luminescent emission.

5.1.1. Core-Shell Systems

Kang et al. [89] published the synthesis of two types of core-shell gadolinium oxide nanoparticles with diameters of 50–60 nm. The gadolinium core was prepared by ap-

plying a modified "polyol" protocol (Figure 9). The average size of the formed particles was 13 nm. The encapsulation of Gd_2O_3 by polysiloxane shell growth was performed by hydrolysis-condensation protocol. The obtained Gd_2SiO_2–NH_2 nanoparticles were then functionalized with two different DOTA (1,4,7,10-tetraazacyclododecane-1,4,7,10-tetraacetic acid) and DO3A-BTA (1,4,7,10-tetraazacyclododeca ane-1,4,7 -trisacetic acid conjugates of benzotriazole) via amide bond formation. The main results were: (1) the synthesized Gd-oxide NPs, Gd_2SiO_2- DO3A, and Gd_2SiO_2-DO2A-BTA showed a high solubility and colloidal stability. (2) The r_1 relaxivities of both NPs were higher than those corresponding low-molecular-weight magnetic resonance imaging contrast agents (MRI CAs). Their r_2/r_1 ratios are close to 1, indicating that both can be used as potential T_1 MRI CAs. (3) Gd_2SiO_2-DO2A-BTA NPs exhibit a strong intracellular uptake property in a series of tumor cell lines and observe significant anticancer characteristics against cell lines such as SK-HEP-1 MDA-MB-231, HeLa, and Hep-3B. (4) Gd_2SiO_2- DO3A and Gd_2SiO_2-DO2A-BTA showed r1 relaxivities higher than that for Gd(DO3A-butrol) atypical small molecule MRI CA.

Figure 9. Functionalization strategies on gadolinium-based oxides.

5.1.2. Functionalization by Non-Covalent Interactions

Ahmad et al. [10] reported the functionalization of ultra-small Gd_2O_3 nanoparticles with poly(methyl vinyl ether-alt-maleic acid) (PMVEMA) polymer (Figure 9). The two carboxylic acid functional groups present in PMVEMA produce a strong interaction among the polymer and Gd_2O_3 NPs through multiple coordination bonds (See Section 3.1.4 for details).

Podgórna et al. [90] reported the synthesis of gadolinium alginate gels nanoparticles (GdNG) with an average size of 110 nm by the reverse phase microemulsion and physical cross-linking method. First, by preparing a reverse-phase microemulsion, Rhodamine fluorescent dye was encapsulated, taking advantage of the super absorption of hydrogels networks. Rhodamine was mixed with freshly prepared GdNG and incubated for 24 h in the dark. Surface modification of GdNG was carried out by layer-by-layer technic (LbL), which consisted of the subsequent absorption of a polycation electrolyte (chitosan) forming multilayer capsules (CHI/GdNG). Other modifications incorporated

the polycation chitosan and the polyanion alginate, alternating positive and negative layers ALG/CHI/GdNG. The main results were: (1) Active compounds could be loaded in GdNG as shown for the absorption of Rhodamine. (2) GdNG, CHI/GdNG, and ALG/CHI/GdNG showed no statistically significant toxic effect in human neuroblastoma cell line SH-SY5Y. (3) It was possible to visualize the GdNG by MR imaging. GdNG reduces the T1 relaxation time compared to the control. (4) GdNG may act as a vehicle to carry hydrophilic drugs for theragnostic applications.

Chaudhary S. et al. [64] reported the synthesis and Gd_2O_3 NPs functionalized with ethylene glycol (EG) by the hydrothermal method starting from $GdCl_3$ and EG. (See Section 3.1.5 for more details). The hydrothermal process has several advantages over other methodologies for synthesizing Gd_2O_3 NPs that generally require very high-temperature reaction conditions and multistep processing.

5.1.3. Functionalization by Chemical Conjugation

Long et al. [91] reported the synthesis of ultra-small gadolinium oxide nanoparticles (UGNPs) with cancer-targeting ability. The UGNPs were grafted with polyacrylic acid (PAA) for biocompatibility and colloidal stability, then conjugated with cancer-targeting arginylglycylaspartic acid (RGD). The functionalization with RGD was carried out by chemical conjugation by amide bond formation. The average size of the formed PAA-UGNPs was 1.8 nm. The RGD-PAA-UGNPs were intravenously administered into the tails of nude model mice with cancer. Accumulation was monitored by magnetic resonance imaging. At the time of the complete collection of the RGD-PAA-UGNPs at the cancer site, the thermal neutron beam was locally irradiated onto the cancer site. The cancer growth was monitored for 25 days. For the first time, the authors reported the successful application of the surface-modified ultra-small gadolinium oxide nanoparticles. Using the cancer model nude mice, the in-vivo gadolinium neutron capture therapy (GdNCT) was demonstrated. The RGD-PAA-UGNPs accumulated selectively at the cancer site and showed GdNCT effect on cancer.

Shen et al. [92] developed a novel blood-brain barrier (BBB)-transportable nanomaterial with an average size of 13.4 nm for high-efficiency theragnostic glioblastoma. The stabilized Gd_2O_3 nanoparticles were synthesized by the wet chemical method using polyacrylic acid (PAA) as a stabilizer. The obtained small gadolinium nanoparticles (ES-GON) were reacted with reductive BSA through an amide bond formation reaction to get ES-GON-rBSA. Lactoferrin (LF) and arginylglycylaspartic acid (RGD) peptides were attached through -COOH and NH_2 groups in the presence of EDC and NHS to generate composite nanoparticles ES-GON-rBSA-LF-RGD. The LF receptor helped ES-GON-rBSA-LF-RGD transport across BBB. Meanwhile, RGD interacts with $\alpha v \beta 3$ integrins targeting brain tumors. ES-GON-rBSA-LF-RGD particles were found to have 13.4 nm average size and negative, superficial charge with assured good blood circulation. The ES-GON-rBSA-FL-RGD2 showed extraordinary relaxivities ($r_1 = 60.8$ mM^{-1}s^{-1}, $r_2/r_1 = 1.1$). Thus, they can be used as a strong T_1-weighted MRI contrast agent, which allows the evaluation and monitoring of tumor therapy. The maximum signal enhancement (ΔSNR) for T_1-weighted 2 MRI of tumors reached up to $423 \pm 42\%$ at 12 h post-injection of 3 ES-GON-rBSA-LF-RGD2, which is much higher than commercial Gd-chelates (<80%).

Sui et al. [93] reported the synthesis of the antifouling ultrasmall Gd_2O_3 NPs modified with PEG and surface coated with zwitterionic cysteine (Cys) for improved MRI (magnetic resonance imaging) of the metastasis lung tumor cells. Solvothermal methods performed the synthesis (Figure 9). The functionalization process was achieved by activating the carboxylic groups in Gd_2O_3 NPs by EDC and NHS in an aqueous solution. Then NH_2-PEG-Mal was added. Gd_2O_3-PEG-Mal was obtained after lyophilization. Afterward, a reaction with Cys was performed to get Gd_2O_3-PEG-Cys NPs. The prepared Gd_2O_3-PEG-Cys-NPs size of 3.2 nm and an r_1 relaxivity of 1.2 mM/s were stable. Gd_2O_3-PEG-Cys-NPs showed acceptable in vitro organ biocompatibility. Besides, it targets specific cancer cells and activates the dual-mode MRI of lung metastasis cancer. PEG-coated Gd_2O_3-PEG

and Gd_2O_3-PEG-Cys-NPs with and without Cys may be performed as the promising T_1-weighted MR imaging.

5.1.4. Coated Gadolinium Oxide Nanoparticles

Yue et al. [94] reported the synthesis of carbon-coated Gd_2O_3 ultra-small nanoparticles core-shell system for medical applications. The first step of synthesis is the preparation of ultra-small Gd_2O_3 nanoparticles in triethylen glycol (TEG). Gd_2O_3 particles were subject to a carbon-coating process in an aqueous solution using dextrose as a carbon source. NPs with an average size of 3.1 ± 1.0 nm were obtained. The NP suspension showed their suitableness for an imaging application. The NPs suspension sample ($r_1 = 16.26$ s^{-1}mM^{-1} and $r_2/r_1 = 1.48$) showed in vivo T_1 MR images of high contrast in mice after intravenous administration. Due to their ultra-small size, the NPs were then excreted through the renal system. Besides, the NP suspension exhibited strong fluorescence in the visible region and fluorescence confocal images on a micrometer scale due to carbon coating on the NP surfaces. The results suggest that the ultrasmall Gd_2O_3@C NPs should be useful as a dual-modal imaging agent in T_1 MRI and FI.

Jamil et al. [95] reported the synthesis of Gd_2O_3 NPs coated with chitosan (Cs) as MRI (Figure 9). The authors evaluated the effect of gamma irradiation on particle size reduction. The synthesis of Gd_2O_3 NPs was conducted by the hydrothermal method starting from $GdCl_3$ 6H$_2$O. Coating process by simply mixing an acidic chitosan solution with Gd_2O_3 NPs. Size reduction was performed via a "one-pot" way by irradiation of Gd_2O_3-Cs using Cobalt-60 at a different dose of gamma irradiation (10, 30, and 40 kGy/h). Particle size was influenced by gamma irradiation. A dose of 10 kGy produced a reduction of particles with spherical morphology from 120 to 45 nm.

Mortezazadeh et al. [96,97] reported the preparation of Gd_2O_3 nanocomposite coated with β-cyclodextrin (CD)-based polyester (PCD) and targeted by folic acid (FA) as a novel targeted MRI contrast agent. PCD-coated Gd_2O_3 NPs (Gd_2O_3/PCD) were prepared by mixing Gd_2O_3 with CD and TEA, forming a stable complex between the OH group from CD and Gd_2O_3. DTPA-DA (Diethylenetriaminepentaacetic dianhydride) was then added. Folic acid was conjugated on the surface of Gd_2O_3/PCD through EDC/NHS amidation using a hydrazine derivative of FA. The prepared nanoparticles were spherical with homogeneous morphology in the 75–90 nm range. PCD as a shell increases biosafety and excludes cytotoxicity risk of Gd_2O_3 when used as MRI contrast agent.

Vahdatkhah et al. [67] reported the synthesis of coated polyvinyl pyrrolidone (PVP) ultrasmall Gd_2O_3 NPs by a microwave-assisted polyol technic. Prepared PVP-coated Gd_2O_3 NPs showed a spherical shape and uniform size of 2.5 ± 0.5 nm (See Section 3.1.6 for more details). The C=O group from PVP interacts directly with either Gd^{3+} ions or Gd_2O_3 by a complexation interaction. The obtained PVP-coated Gd_2O_3 NPs showed an enhanced T_1-weighted signal intensity and an r_1/r_2 ratio close to the unit, making them superior for positively contrasted T1-weighted images.

Kumar et al. [98] reported the reverse micelle-mediated synthesis of multifunctional dextran (dex) coated Gd_2O_3 NPs carrying rose Bengal dye for the simultaneous purpose of magnetic resonance (MR) and optical imaging (OI). Particles worked as CA in MRI, and the presence of RB ensures their application for optical tracking in biological systems. Biocompatibility and non-toxicity NP were coated with dex. Dex also acts as a conjugator to attach RB to the NPs. The synthesis was performed by water-in-oil microemulsion mediated synthesis, starting from $Gd(NO_3)_3$ as starting material. Obtained particles were found to be spherical with an average diameter of 17 nm; highly dispersed in size and shape.

5.2. Gadolinium-Based Oxysulfides

5.2.1. PEGylation

Santelli et al. in 2018 [99] reported the synthesis and PEGylation of Gd_2O_2S:Eu^{3+} nanoparticles as nanoplatforms for multimodal bioimaging. Synthesis was conducted by oxidation of hydroxycarbonates by annealing at 750 °C for 4 h. Treatment with sulfur at

850 °C under argon atmosphere generated $Gd_2O_2S:Eu^{3+}$ nanoparticles. PEGylation was achieved by mixing $Gd_2O_2S:Eu^{3+}$ nanoparticles with PolyEthylene Glycol (PEG) in water. The mixture was sonicated for 1 h and stirred at 50 °C for 24 h, followed by sonication. PEGylation prevents any aggregates formation. TEM analysis revealed that the obtained nanoparticles showed a spherical shape (150 nm dimeter).

5.2.2. Core-Shell Systems

Osseni and co-workers [100] reported the synthesis of $Gd_2O_2S:Eu^{3+}$ nanoparticles (NPs), from hydroxycarbonate precursor precipitation followed by sulphuration in a H_2S/Ar atmosphere at 750 °C. The surface of oxysulfide NPs was modified by an amino-silica or by a mesoporous silica shell (thickness 10–15 nm). Europium-doped gadolinium hydroxycarbonates were synthesized from nitrate precursors in water and ethanol, following a procedure based on Matijevic and Hsu's reports [75]. The obtained hydroxycarbonates were sulphurated by a solid-gas reaction at 750 °C under an Ar–H_2S atmosphere. $Gd_2O_2S:Eu^{3+}$ particles were coated with silica using the hydrolysis of tetraethoxysilane (TEOS), following the Stöber process [101]. Briefly, $Gd_2O_2S:Eu^{3+}$ nanoparticles were dispersed in 1-propanol by sonication for 2 h. Then ammonia (morphological catalyzer), de-ionized water (hydrolytic reagent) and TEOS were added into the mixture. The mixture was vigorously stirred at 40 °C for 2 h. 3-aminopropyltrimethoxysilane (APTMS) was then added to the suspension. The resulting particles were washed with 1-propanol.

The core-shell structured $Gd_2O_2S:Eu^{3+}@mSiO_2$ (m for mesoporous) nanocomposites were also obtained via a modified Stöber sol-gel process [102]; $Gd_2O_2S:Eu^{3+}$ nanoparticles were dispersed in 1-propanol by sonication. Ammonia de-ionized water, cetyltrimethylammonium bromide (CTAB) (structure-directing agent), and TEOS were added into the mixture, which was vigorously stirred at 40 °C for 6 h. The products were collected by centrifugation, washed with 1-propanol, and dried. The (CTAB) was removed from the pores by calcination.

Authors conclude that coated $Gd_2O_2S:Eu^{3+}$ core with a dense thin amino-silica shell can be grafted with biomolecules, such as streptavidin. The $Gd_2O_2S:Eu^{3+}@SiO_2$-APTMS nanoplatform could be used as a luminescent nanoprobe and/or MRI contrast agent. Meanwhile, a thick mesoporous silica coating on the scintillator core ($Gd_2O_2S:Eu^{3+}@mSiO_2$), could be used as a nano-tank for any drug loading to form a trackable drug delivery system. Some tests on NIH_3T_3 mouse living cells proved that the $Gd_2O_2S:Eu^{3+}$ nanophosphor can be easily internalized and imaged by epifluorescence microscopy, with excitation in the NUV (365 nm), no cytotoxic effects were observed in living cells. According to the authors, spherical monodispersed $Gd_2O_2S:Eu^{3+}$ nanophosphor could be considered as a better luminescent biolabel than the corresponding oxide or fluoride nanoparticles.

6. Biological Applications on Gadolinium-Based Particles

Gadolinium-based particles have been reported for promising bio-applications (Figure 10) due to their interesting optical properties, highlighted physicochemical characteristics, combined with low cytotoxicity and high photosensitivity [103]. Because of their high longitudinal relaxivities and small r_2/r_1 ratios, Gd_2O_3 and Gd_2O_2S NPs are used for magnetic resonance imaging (MRI), dual-modal imaging, tissue labeling, immunosensing, and photodynamic therapy (PDT) [17,104,105]. Moreover, the surface of upconverting nanoparticles can be functionalized and then conjugated with biological molecules (such as proteins, peptides, antibodies, drugs, and genes) to be delivered in target cells. Gadolinium-based nanoparticle systems are currently under evaluation for several biological applications. Table 1 summarizes some relevant works published on this topic.
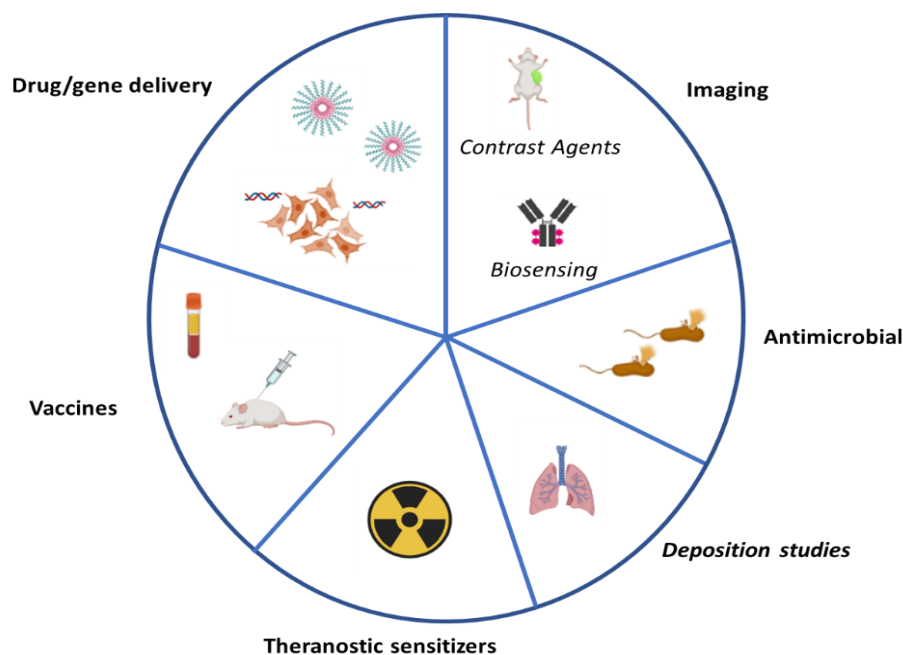
Figure 10. Main biological applications of gadolinium-based oxides. Created with https://biorender.com/ (accessed on 7 September 2021).

6.1. Imaging

6.1.1. Gd_2O_3 Particles

Bridot et al. [106], synthesized hybrid nanoparticles by encapsulating Gd_2O_3 cores within a polysiloxane shell that carries organic dyes and the outer part with PEG. Results revealed longitudinal proton relaxivities higher than the contrast agents commonly used for MRI. These particles can be followed up by fluorescence imaging. Moreover, these do not have a significant accumulation in the lungs or liver of Female Swiss nude mice. Maalej et al. [107] developed Gd_2O_3 doped by europium (Eu) (2% to 10%) nanoplatelets through the polyol chemical method. Microscopy assays revealed a crystalline cubic structure of the Gd_2O_3 matrix. Gd_2O_3:Eu^{3+} exhibited a strong red luminescence signal around 612 nm. Therefore, these nanoplatelets can be exploited in labeling biological materials for fluorescence microscopy applications. Faucher et al. [108] reported a new, fast, and efficient one-pot Gd_2O_3 synthesis method through which they obtained ultrasmall (1.3 nm) PEGylated nanoparticles. These PEG-Gd_2O_3 nanoparticles were stable in aqueous media and had high longitudinal relaxivities. These also allowed the visualization of labeled cells implanted in vivo (mice brains). Nichkova et al. [109], synthesized europium doped gadolinium oxide (Eu:Gd_2O_3) nanoparticles by spray pyrolysis, and then they covered these with antibody (IgG) molecules through physical adsorption. Results showed that Gd_2O_3:Eu^{3+} is an excellent matrix for antibody immobilization. Besides, the immobilized antibodies hold their biological activity and specificity so that these nanoparticles can be used as fluorescent markers in a variety of immunosensing applications. Gordon et al. [31] obtained lanthanide Gd_2O_3 nanoparticles by gas-phase condensation method. They used three dopants Tb^{3+}, Dy^{3+}, Eu^{3+}, which provide strong emission lines. Results indicated that dopant combinations with long lifetimes and typical excitation wavelength could be used for multicolor immunoassays. Chen et al. [8], synthesized terbium-doped gadolinium oxide (Gd_2O_3:Tb) NPs, assessing different concentrations of Tb. The study revealed the optimum Tb doping concentration at 1%.

On the other hand, microscopy images showed spherical NPs with excellent crystallinity. Cell viability assays revealed no significant cytotoxic effect. Cellular fluorescence imaging in S18 cells clearly showed the green fluorescence from Gd_2O_3:Tb^{3+}. An in vivo

MRI experiment in BALB/c nude mice demonstrated that these NPs could provide a clear contrast enhancement for the tumor within a suitable time.

Dosev et al. [110] synthesized Europium-doped gadolinium oxide (Eu:Gd_2O_3) nanoparticles by spray pyrolysis with a size distribution from 5 nm to 500 nm. Laser-induced fluorescent spectroscopy showed a main peak at 612 nm. These NPs were coated with avidin. Biotinylated Bovine Serum Albumin (BSA-b) was patterned on a silicon wafer and then incubated in a solution containing the avidin-coated nanoparticles. Results from fluorescent microscopy revealed that the nanoparticles were organized into designated structures. The fluorescent pattern did not suffer any photobleaching during the observation period, proving the suitability of Eu:Gd_2O_3 nanoparticles as fluorescent labels with large excitation times. Fang et al. [111] synthesized ultra-small Gd_2O_3 nanoparticles (average size of 2.9 nm) coating with polyvinyl pyrrolidone (PVP). These NPs (Gd_2O_3-PVP) showed an improved longitudinal relaxivity r_1 of 12.1 mM^{-1} s^{-1} at 7 T, around three times that of the Magnevist (a commercial contrast agent). In vitro assays revealed low cytotoxicity of Gd_2O_3-PVP within preclinical dosage. In vivo, MR imaging in SCID mice showed an enhancement signal in the liver and kidney with a long blood circulation time.

Mekuria et al. [112] encapsulated (Gd_2O_3) nanoparticles in PAMAM Dendrimer Templates (G4.5-Gd_2O_3-PEG), and they compared them with the clinically used Gd-DTPA contrasting agents, the longitudinal relaxivity (r1) of G4.5-Gd_2O_3-PEG NPs was 53.9 s^{-1} mM^{-1} at 7T, 4.8 times greater than that of Gd-DTPA. Besides, G4.5-Gd_2O_3-PEG showed better in vitro biocompatibility when evaluated with macrophage cell line RAW264.7. In addition, BALB/c female mice in vivo assays revealed enhanced signals in the intestines, kidney, liver, bladder, and spleen. These results demonstrate that G4.5-Gd_2O_3-PEG NPs could be an alternative approach as dual MRI contrasting agents. Mastrogiacomo et al. [113], synthesized gadolinium(III) oxide nanoparticles by the polyol method and functionalized their surface with bisphosphonate (BP) derivative. The CPC-GBCAs-BP nanoparticles were stable in an aqueous solution. The nanocomposite was implanted in rats. The dual-modality nanoparticle probe allowed the visualization of the implanted cement up to 8 weeks after the implant. No adverse effects were found on the surrounding bone tissues.

6.1.2. Gd_2O_2S Particles

Gadolinium oxysulfide nanoparticles have also been reported as potential imaging agents. Osseni et al. [45] reported the synthesis of gadolinium oxysulfide nanoparticles doped with Eu^{3+}, Er^{3+} or Yb^{3+}, via a hydroxycarbonate precursor precipitation route followed by a sulphuration process. Results showed that Gd_2O_2S:Eu^{3+} NPs strongly absorbed X-ray or near UV (363 nm) and re-emit a red light with high intensity. Later, these systems were evaluated in studies of fluorescence microscopy, MR imaging, and X-ray tomography. The results showed that the red emission line at 670 nm of the Gd_2O_2S:Er^{3+}:Yb^{3+} system could be applied efficiently for deep in-vivo fluorescence imaging. Finally, the MTT assay was used to evaluate the cytotoxicity of different concentrations of the NPs on MDA-MB231 cells. The cytotoxicity of particles at 100 μg/mL concentration was negligible [26]. In a similar study, Santelli et al. [99] presented Gd_2O_2S:Eu^{3+} nanoparticles as a candidate for imaging techniques as they are detectable by (1) magnetic resonance (MRI), (2) X-ray, and (3) photoluminescence imaging [27]. This type of NPs has also been used in photodynamic therapy (PDT).

Rosticher et al. [114] developed Gd_2O_2S: Eu^{3+}, Ti^{4+}, Mg^{2+} nanoprobes for multimodal imaging. Gd_2O_2 nanoparticles were synthesized using a three-step hydrothermal route. These show an afterglow in the red range at 620 nm and a relaxivity corresponding to r2/r1 ratio of 1.28. The nanoparticles exhibited both persistent luminescence and paramagnetic properties. Hassani et al. [14], synthesized a Gadolinium oxysulfide phosphor doped with trivalent terbium (Gd_2O_2S:Tb^{3+}) using homogenous urea precipitation followed by sulfurization at 800 °C under argon atmosphere. The maximum light output and contrast were observed for the layer with a thickness of 193 μm. Emitting green light from the phosphor layer confirms its luminescence property.

Table 1. A summary of the most used gadolinium-based nanoparticles in the biomedical field.

Particle	Synthesis Strategy	Size and Morphology	Biological Application	Results	Ref.
Gd_2O_3	Modified polyol protocol	Nanospheres	Imaging	Longitudinal proton relaxivities higher than the contrast agents commonly used for MRI	[99]
Gd_2O_3:Eu^{3+}	Polyol	Nanoplatelets	Imaging	Doping with Eu exhibits strong PL spectra, especially at 612 nm	[100]
Gd_2O_3	One-pot	Ultrasmall nanospheres	Imaging	NPs showed high longitudinal relaxivities. These allowed the visualization of labeled cells implanted in vivo	[101]
Gd_2O_3:Eu^{3+}	Spray pyrolysis	Quasi-spherical	Imaging and immunosensing	Excellent matrix for antibody immobilization	[102]
Gd_2O_3 doped with Tb^{3+}, Dy^{3+}, Eu^{3+}	Gas-phase condensation	Fluffy morphology	Imaging and immunosensing	Strong emission lines and long lifetimes. Dy^{3+} was the most sensitive to concentration quenching	[31]
Gd_2O_3:Tb^{3+}	Spherical	Spherical	Imaging	Cellular fluorescence imaging in S18 cells clearly showed the green fluorescence from Gd_2O_3:Tb intracellular	[8]
Gd_2O_3:Eu^{3+}	Spray pyrolysis	Nearly-spherical	Imaging	NPs do not suffer any photobleaching and show significant excitation times	[103]
Gd_2O_3	Organic synthesis	Ultrasmall nanospheres	Imaging	Improved longitudinal relaxivity r1 of 12.1 mM^{-1} s^{-1} at 7 T	[104]
Gd_2O_3	Organic synthesis	Spherical	Imaging	NPs exhibited a longer longitudinal relaxation time (T1) and better biocompatibility with macrophage cell line	[105]
Gd_2O_3	Polyol	Spherical	Theranostic sensitizers	The sensitizer enhancement ratio at the 10% survival level and elicited an increase in hydroxyl radical production, which led to DNA damage and cell cycle arrest.	[114]
Gd_2O_3	Simple precipitation	Spherical	Antimicrobial agents	NPs had a potent antimicrobial effect against gram-negative and gram positives bacteria	[16]
Gd_2O_3	Sonication technique	Spherical	Antimicrobial agents	NPs had antimicrobial and antifungal effects	[108]
Gd-NGO	Organic synthesis	Dendrimer	Drug and micro RNA delivery	NPs were able to deliver EPI and Let-7g miRNA into cells to destroy the DNA and then inhibited the cancer cell growth	[109]
Gd_2O_3	Fungus based approach	Quasi-spherical	Drug delivery	Bioconjugation with taxol was potent in killing tumor/cancer cells	[70]
Gd_2O_3:Eu^{3+}	High temperature solvothermal	Small triangular nanoplates	Drug delivery	Efficient delivery of drugs to the nuclei of cancer cells (HeLa and KB) with a high cytotoxic effect	[111]

Table 1. *Cont.*

Particle	Synthesis Strategy	Size and Morphology	Biological Application	Results	Ref.
$Gd_2O_3:Eu^{3+}$	Sol-gel process	Nanospheres	Drug delivery	The nanocomposite system exhibited more significant cytotoxicity compared to Dox free	[112]
Gd_2O_3	Simple wet-chemical route	Rod-shaped	Drug delivery and imaging	Nanorods were internalized by cells more quickly than the control (DOX free) and displayed more cell cytotoxicity. Furthermore, these can serve as contrast agents for MRI	[17]
$Gd_2O_3:Eu^{3+}$	Flame pyrolysis	Spherical	Deposition studies	The dose of deposited particles was significantly greater in the juvenile rats at 2.22 ng/g body weight. The NPs did not show toxicity in any organ.	[18]
$Gd_2O_3:Eu^{3+}$	Spray flame pyrolysis	Quasi-spherical	Deposition, clearance, and translocation	NPs were detected in all the studied organs at low ppb levels; 59% of the particles remained in the lung.	[113]
$Gd_2O_3:Tb^{3+}/Er^{3+}$	Hydrothermal	Spherical	Vaccines	Microparticles have shown an enhanced humoral (with a Th2-polarization) response compared with the control groups.	[19]
Gd_2O_3	Polyol	Spherical	Imaging	The combination of NPs with CPC gives an injectable material that allowed the visualization of the implanted cement up to 8 weeks after implant	[115]
$Gd_2O_2S: Er^{3+}:Yb^{3+}$	Hydroxycarbonate precursor precipitation.	Spherical	Imaging	NPs under infrared excitation ($\lambda ex = 980$ nm) show mainly red emission ($\approx$650–680 nm). Consequently, they are more specifically designed for in vivo deep fluorescence imaging	[45]
$Gd_2O_2S:Eu^{3+}$	Hydroxycarbonate precursor precipitation	Spherical	Imaging	NPs demonstrated no toxic effects on whole organisms and their long-lasting tracking aptitude as well as their potential use as multimodal cell trace	[101]
$Gd_2O_2S: Eu^{3+}, Ti^{4+}, Mg^{2+}$	Hydrothermal	Nanoprobes	Imaging	NPs exhibited both persistent luminescence and paramagnetic properties.	[50]
$Gd_2O_2S:Tb^{3+}$	Urea homogenous precipitation	Hexagonal structure	Imaging	Emitting of green light from phosphor layer confirms its luminescence property.	[14]

6.2. Antimicrobial Effects Gd_2O_3 Particles

Ashima et al. [16] synthesized spherical Gd_2O_3 nanoparticles and coated them with L-ascorbic acid via a simple precipitation route. These nanoparticles did not show toxicity when they were evaluated in vitro. Their antimicrobial effect was tested on *E. coli*, *S. aureus*, and *S. Typhimurium* strains. The Asc-Gd_2O_3 nanoparticles had a potent antimicrobial effect against gram-negative and gram-positive bacteria. The same report showed that Gd_2O_3

nanoparticles coated with L-lysine amino acid had antimicrobial and antifungal effects when tested on two bacterial strains, *Escherichia coli* and *Staphylococcus aureus*, and two fungal strains, *Candida albicans* and *Candida glabrata*. The minimal inhibition concentrations (MIC) were 8 μg mL^{-1} for bacterial strains and 16 μg mL^{-1} for fungal strains. Cell viability assays revealed non-toxicity on HaCaT cells [115].

6.3. Drug/Gene Delivery
Gd$_2$O$_3$ Particles

Yang et al. [116] produced nanoparticles of poly(amidoamine) dendrimer-grafted gadolinium-functionalized nanographene oxide and evaluated them as effective carriers to deliver both chemotherapeutic drugs and particular gene-targeting agents such as microR-NAs (miRNA) to cancer cells. The authors reported a high transfection efficiency in human glioblastoma (U87) cells, observing that gadolinium-functionalized nanographene oxide NPs could deliver EPI and Let-7g miRNA into cells to destroy the DNA then inhibited the cancer cell growth. Thus, these NPs can be used as a promising non-viral vector for chemo-gene therapy in future clinical applications. On the other hand, Yoo et al. [117] reported doxorubicin (Dox) delivery system based on a gadolinium hydroxide (Gd(OH)$_3$) nanorod. The synthesis was achieved in manganese (Mn) ions and Dox to produce the Gd(OH)$_3$:Mn centerdotDox nanocluster structure. The nanorod did not show in vivo toxicity; moreover, the nanocluster was able to release Dox in a sustained and pH-dependent manner. The system was tested on MDA-MB-231 breast cancer cells, observing that the released Dox was cytotoxic and able to inhibit the proliferation of cancer cells. Khan et al. [69] synthesized Gd$_2$O$_3$ nanoparticles by using the thermophilic fungus *Humicola* sp at 50 °C. The NPs were highly stable and well-dispersed. These NPs were bioconjugated with taxol (an anticancer drug), and biodistribution studies showed that Gd$_2$O$_3$ nanoparticles accumulated in the liver, heart, and kidneys, and cleared through urine within 45 min. This particular bioconjugation is thus proposed as a viable approach to develop potent agents to kill malignant cells. Saha et al. [118] reported small Eu:Gd$_2$O$_3$ triangular nanoplates synthesized via a high-temperature solvothermal technique. The surface was coated with polyacrylate and then modified with free thiols to specifically attach daunorubicin and curcumin drugs. Both drugs showed high loading (~69% for daunorubicin and ~75% for curcumin). Fluorescence imaging assays confirmed the efficient delivery of medicines within the nuclei of cancer cells (HeLa and KB) with a high cytotoxic effect.

Xu et al. [119] encapsulated Gd$_2$O$_3$:Eu^{3+} nanospheres with nonporous silica and a further layer of ordered mesoporous silica via a sol-gel process. Doxorubicin hydrochloride (DOX) was loaded in the Gd$_2$O$_3$:Eu^{3+}@nSiO$_2$@mSiO$_2$ composites to evaluate their performance as drug nanocarriers. In vitro, HeLa cells assay demonstrated that DOX is shuttled from loaded composites into the cell and uptaken by endocytosis. DOX released from core-shell-shell nanocomposites showed more significant cytotoxicity compared to the DOX control. Besides, MTT assay revealed low cytotoxicity of the nanocarriers in fibroblasts.

Zhou et al. [17] developed Eu^{3+}-doped mesoporous Gd$_2$O$_3$ nanorods by a simple wet-chemical route, the materials were modified with polyethylene glycol (PEG) to load the doxorubicin hydrochloride (DOX). TEM images showed monodisperse rod-shaped Eu^{3+}-doped Gd(OH)$_3$ precursor with a length of 160 nm and diameters of 40 nm. In vitro cytotoxicity of these nanorods revealed no cytotoxic effects in the BXPC cells. However, release trials showed that Gd$_2$O$_3$:Eu@PEG-DOX was internalized by cells more quickly than the control (DOX free) and displayed higher cytotoxicity. Furthermore, the multifunctional nanorods served as contrast agents for MRI.

6.4. Deposition Studies
Gd$_2$O$_3$ Particles

Das et al. [18] developed europium-doped gadolinium oxide nanoparticles (Gd$_2$O$_3$:Eu^{3+}) and assessed deposition in the developing rat lung. Neonatal, juvenile, and adult rats

were exposed to 380 µg/m^3 dose of NPs for 1 h. Mass spectroscopy studies showed that the amount of Gd_2O_3:Eu^{3+} deposited in the lungs was more significant in juvenile rats at 2.22 ng/g body weight than for adult and neonate rats (1.47 ng/g and 0.097 ng/g, respectively). The NPs did not show acutely toxic or inflammatory. In the lung tissue of juvenile and adult rats, the same mass of deposited NPs was found. In a similar study, Abid et al. [120] investigated the deposition, clearance, and translocation of (Gd_2O_3:Eu^{3+}) in the lungs of the mouse. The particles were intratracheally deposited into the mouse lung; after 24 h, organs were harvested and analyzed. Inductively coupled plasma mass spectrometry (ICP-MS) analysis revealed that 59% of NPs remained in the lung. In addition, a significant amount of NPs was found in the gastrointestinal tract and feces, suggesting fast clearance mechanisms. The nanoparticle systems reported in these works could be used in deposition, transport, and clearance studies of NPs from the lung. These reports demonstrate the utility of novel lanthanide-based nanoparticles to study in vivo inhaled particle deposition. They also have important implications for nanoparticles delivery to the developing lung either as therapies or as a portion of particulate matter air pollution.

6.5. Vaccines
Gd_2O_3 Particles

Ortega-Berlanga et al. [19] synthesized carriers based on Gd_2O_3:Tb^{3+}/Er^{3+} particles obtained by hydrothermal method, then doped with APTES to anchor a predict antigenic B-cell epitope from the E protein of Zika Virus (ZK2). Results showed a stable colloidal system with a high loading capacity (0.480 µg of ZK2 peptide/µg of microparticles). These microparticles were administered to mice subcutaneously, showing an enhanced humoral response compared with the control groups. In addition, IgG subclass analysis revealed a Th2-polarization. This study supports the use of Gd_2O_3 particles as microcarriers for immunization applications, representing a valuable tool for developing new nanovaccines based on the induction of humoral responses.

6.6. Theranostic Sensitizers
Gd_2O_3 Particles

Li et al. [121] synthesized ultra-small gadolinium oxide nanocrystals (GONs) via the polyol method, and they investigated their radiosensitizing effects in non-small-cell lung cancer (NSCLC) cells under X-ray irradiation. Results showed that GONs induced radical hydroxyl production and oxidative stress in a dose/concentration-dependent. Furthermore, the GONs promoted cytostatic autophagy in NSCLC cells under X-ray irradiation.

7. Concluding Remarks and Prospects

The analysis of the literature reveals that both oxides and oxysulphides systems have been used recently as contrast agents, detection agents, antimicrobial agents, transport systems (RNA, proteins, peptides, and drugs), and in the formulation of nanovaccines prototypes (see Table 1). Several authors agree that even despite a large number of nanoparticles available for these applications, the main attributes of gadolinium-based compounds make them attractive candidates [5]. In the last decade, the Gd_2O_3 has been extensively used for biomedical applications, which is attributed to these reasons: (1) The easier production of Gd_2O_3 than Gd_2O_2S, (2) the chemical modification of the Gd_2O_3 surface is more accessible than Gd_2O_2S, and (3) the multifunctionality of Gd_2O_3 as a contrast agent and therapeutic agent [122]. However, advances in the synthesis methods have allowed a decrease in the particle size and modulation of the shape of the Gd_2O_2S. In the same biomedical applications, better results are expected due to the superior optical properties [5].

According to the examined studies, the synthesis methods to produce Gd_2O_3 and Gd_2O_2S can be classified into two types: (1) a single-step procedure, and (2) the two or more steps procedure. The single-step procedure includes all direct techniques (sonic-chemical reaction, solid-state reaction, the sol-gel method, polyol method, etc.) that induce the

formation of oxides and oxysulfides through redox reactions [7–10,53,68]. These methods can produce nano- or micro-particles with modulable size and shape. However, it is also important to note that some of these methods produce compounds with low crystallinity and generate organic by-products that are difficult to remove. Eventually, these undesired products affect the particles' biological interaction and optical properties, limiting their application [123,124].

The two or more steps procedure (or sulfuration processes) is a route that requires freshly prepared carbonates, hydroxycarbonates, or oxides as precursor material to form the oxysulfides [77]. This process includes the solid-state sulfidation reaction. Its main advantage is that particles used as precursors with a specific shape and size can be utilized without any change in morphology, particle size, or defects on the particle surface [4,20]. Furthermore, it has been seen that colloidal systems prepared with particles obtained with this technique seem to be more chemically and optically stable without any contamination by organic compounds [4,77].

Current literature also reveals that the chemical modification of the Gd_2O_3 surface is more common compared to Gd_2O_2S. This fact is mainly due to -OH groups exposed on the Gd_2O_3 surface, which are more chemically active under less extreme conditions, this has allowed the formation of chemical bonds to anchor different biomolecules such as APTES [74], DO_3A-BTA [89], PMVEMA [10], EG [64], PEG [93], PAA [91], among others. In the particular case of Gd_2O_2S, the gadolinium ion is wholly coordinated by four oxygen and three sulfur atoms. This fact means that the sulfur exposed on the particle surface could not quickly induce new bonds [125]. To meet these functionalization challenges, new strategies have been developed to modify the particle surface. For instance, Ai et al. [48] synthesized Gd_2O_2S:Eu functionalized with polyethylene glycol (Gd_2O_2S:Eu@PEG) to later anchor a potent [89]Zr oxalate. Moreover, the strategy reported by Chen et al. [126] synthesized Gd_2O_2S:Tb and Gd_2O_2S:Eu nanocapsules with a silica core and functionalized them with styrenesulfonate sodium (PSS) and poly (allylamine hydrochloride) (PAH) for the release of Doxorubicin (DOX).

The multifunctionality of Gd_2O_3 has positioned it as a helpful oxide. However, it is crucial to consider that the Gd_2O_2S matrix has some other qualities that make it attractive. For example, inserting sulfur into the Gd_2O_3 matrix produces changes in the crystal field and improves transitions in the 4f energy levels of the lanthanides. This fact makes the Gd_2O_2S matrix optically more efficient compared to Gd_2O_3. Some works have reported a photon conversion efficiency of Gd_2O_2S greater than that of Gd_2O_3 in approximately 60,000 visible photons/MeV for Gd_2O_2S:Tb, and Gd_2O_2S:Eu, against 40,000 visible photons/MeV for Gd_2O_3:Eu [127]. Our group also observed that the photoluminescent emission is higher in Gd_2O_2S:Tb compared to Gd_2O_3:Tb due to a notable increase in the efficiency of the radiative 4f-4f transitions of Tb^{3+} ions [77]. Additionally, it has been demonstrated that Gd_2O_2S:Eu shows high paramagnetic properties at room temperature with similar magnetic susceptibility and similarly good MRI T_2 relaxivities to Gd_2O_3, but the sulfur increases the radioluminescence intensity and shifts the spectrum [126]. In summary, the recent works on oxysulfides make them a very promising matrix for biomedical and technological applications. Thus, it is expected that the application of oxysulfides will be great as that of oxides.

Additionally, it is important to comment on the challenges and prospects. For example, further work is necessary to explain the effect of the shape and surface energy on the optical and magnetic properties of the particle. This fact is fundamental; our group observed that the intensity of the luminescent emission in oxysulfide is dependent on the surface energy, which means the higher the energy, the higher the emission intensity [77]. However, Wang et al. [128] observed a different effect, finding that luminescent intensity in lanthanide-based crystals is affected by surface defects, impurities, ligands, and solvents. The size also plays an important role in the optical properties. The classic theories, such as quantum confinement and surface plasmon resonance related to the optical properties

of semiconductor and metal nanoparticles suggest a size-dependent luminescence [129]. However, experimental evidence has not been conclusive.

The use of rare-earth-based nanoparticles for different biological applications, including molecular and cell biology, in vitro and in vivo assay, has been demonstrated for several research groups [99,101–105]. An additional advantage is that rare-earth-based nanoparticles can be easily functionalized with specific functional groups to target biomolecules. Besides, their intrinsic optical properties allow them to be used as contrast agents in imaging. Some reports of gadolinium-based oxides for drug/gene demonstrate their applicability for delivery of biological molecules or as vaccine antigen carriers. As mentioned, NPs functionalization is crucial for biological applications because it assures good particle dispersion and stability in the selected media or their innocuity for in vivo experiments. Functionalization strategies include hybridization with reactive groups such as amino, carboxylates, thiols, or aldehydes to promote, in a second step, the coupling with biomolecules of interest (antibodies, peptides, among others). Their optical properties (high photoluminescence, high photostability, blinking absence, extremely narrow emission lines, significant stokes shifts, and long lifetimes) and low cytotoxicity make them suitable to replace organic dyes or quantum dots in all their reported applications.

Oxide and oxysulfide NPs have been primarily evaluated in vitro, and some reports have shown the toxicity of gadolinium oxide/oxysulfide particles on in vivo systems [20,104]. However, much work is still to be done in this area. According to the FDA, gadolinium-based contrast agents increase the risk for Nephrogenic Systemic Fibrosis (NSF) [130]. Nevertheless, the potential toxicity of nanoparticles depends on their constituent materials and the physicochemical properties of their surface coating and particle size. A clinical trial report is currently performed in AGuIX® (Activation-and-Guidance by Irradiation X) NPs, which are 5 nm theranostic nanoparticles formed by a polysiloxane core surrounded by cyclic ligands of gadolinium derived from DOTA (1,4,7,10-tetraazacyclododecane acid-1,4,7,10-tetraacetic acid) and covalently attached to a polysiloxane core. AGuIX® was designed to enhance both radiotherapy treatment and MRI contrast. Several preclinical studies have demonstrated that the presence of AGuIX® NPs inside the tumor during radiotherapy enhances radiotherapy's efficacy, leading to more prolonged survival than radiotherapy treatment [131]. Recently, Verry et al. [132] reported the protocol NANO-RAD (NCT02820454), a phase 1 trial in patients with brain metastases that are not eligible for surgical resection. The principal objective of the test is to investigate the safety, tolerability, and side effects of the AGuIX® NPs. The studies on this protocol suggest that AGuIX gadolinium nanoparticles, after a single intravenous injection, can enhance the image of all metastases and increase the efficiency of the irradiation. This is the first example of gadolinium oxide nanoparticles used in the clinic for radiosensitization after intravenous administration. AGuIX® demonstrates the important impact of gadolinium-based nanoparticles as an alternative for cancer treatment and shows the scientific challenges of improving gadolinium-based particles' safety and efficacy for biomedical applications.

Author Contributions: Conceptualization: B.O.-B. and G.P. Writing—Original Draft: B.O.-B., L.B.-M., L.H.-A., C.d.A.-O. and G.P. Investigation: B.O.-B., L.B.-M., C.d.A.-O., L.H.-A. and G.P. Writing—Review & Editing: B.O.-B., L.B.-M., L.H.-A., C.d.A.-O. and G.P. Review & Editing: S.R.-M. and G.P. Supervision: S.R.-M. and G.P. Visualization, Project administration, Funding acquisition: G.P. All authors have read and agreed to the published version of the manuscript.

Institutional Review Board Statement: Not applicable.

Informed Consent Statement: Not applicable.

Data Availability Statement: The study does not report new data.

Conflicts of Interest: The authors declare no conflict of interest and agree with the manuscript.

References

1. Escribano, P.; Julián-López, B.; Planelles-Aragó, J.; Cordoncillo, E.; Viana, B.; Sanchez, C. Photonic and Nanobiophotonic Properties of Luminescent Lanthanide-Doped Hybrid Organic–Inorganic Materials. *J. Mater. Chem.* **2007**, *18*, 23–40. [CrossRef]
2. Yang, M.; Gui, Q.; Ma, J.; Qi, L.; Bao, B.; Huang, Y. Upconversion Nanotubes with Tunable Fluorescence Properties Based on $Gd_2O_2S:Ln^{3+}$ (Ln^{3+} = Yb^{3+}, Er^{3+}) and Derivatives for Photodynamic Therapy. *IET Nanobiotechnol.* **2020**, *14*, 347–356. [CrossRef]
3. Guo, T.; Lin, Y.; Li, Z.; Chen, S.; Huang, G.; Lin, H.; Wang, J.; Liu, G.; Yang, H.-H. Gadolinium Oxysulfide-Coated Gold Nanorods with Improved Stability and Dual-Modal Magnetic Resonance/Photoacoustic Imaging Contrast Enhancement for Cancer Theranostics. *Nanoscale* **2017**, *9*, 56–61. [CrossRef]
4. Del Angel-Olarte, C.; Hernández-Adame, L.; Mendez-Blas, A.; Palestino, G. Eu^{3+}/Yb^{3+} Co-Doped Gadolinium Oxysulfide Upconverting Nanorods: Morphological, Physicochemical and Optical Evaluation. *J. Alloys Compd.* **2019**, *787*, 1032–1043. [CrossRef]
5. Larquet, C.; Carenco, S. Metal Oxysulfides: From Bulk Compounds to Nanomaterials. *Front. Chem.* **2020**, *8*, 179. [CrossRef]
6. Leiro, V.; Parreira, P.; Freitas, S.C.; Martins, M.C.L.; Pêgo, A.P. Chapter 2-Conjugation Chemistry Principles and Surface Functionalization of Nanomaterials. In *Biomedical Applications of Functionalized Nanomaterials*; Sarmento, B., das Neves, J., Eds.; Micro and Nano Technologies; Elsevier: Amsterdam, The Netherlands, 2018; pp. 35–66, ISBN 978-0-323-50878-0.
7. Perdigon-Lagunes, P.; Estevez, O.; Zorrilla, C.; Gomez, A.; Herrera-Becerra, R. Alkaline Tannin Assisted Synthesis of β-Gd and Gd_2O_3 nanoparticles at Room Temperature. *Appl. Phys. A* **2018**, *124*, 565. [CrossRef]
8. Chen, F.; Chen, M.; Yang, C.; Liu, J.; Luo, N.; Yang, G.; Chen, D.; Li, L. Terbium-Doped Gadolinium Oxide Nanoparticles Prepared by Laser Ablation in Liquid for Use as a Fluorescence and Magnetic Resonance Imaging Dual-Modal Contrast Agent. *Phys. Chem. Chem. Phys.* **2014**, *17*, 1189–1196. [CrossRef]
9. Niftaliev, S.I.; Kuznetsova, I.V.; Saranov, I.A.; Zhundrikova, T.V.; Lygina, L.V.; Tuneekov, V.Y.; Chislova, I.V.; Zvereva, I.A. Synthesis of Nanosized Gadolinium Oxide. *Glass Phys. Chem.* **2019**, *45*, 232–237. [CrossRef]
10. Ahmad, M.Y.; Ahmad, M.W.; Yue, H.; Ho, S.L.; Park, J.A.; Jung, K.-H.; Cha, H.; Marasini, S.; Ghazanfari, A.; Liu, S.; et al. In Vivo Positive Magnetic Resonance Imaging Applications of Poly(Methyl Vinyl Ether-Alt-Maleic Acid)-Coated Ultra-Small Paramagnetic Gadolinium Oxide Nanoparticles. *Molecules* **2020**, *25*, 1159. [CrossRef]
11. Trinh, L.H.; Hoa, T.T.; Van Hieu, N.; Cuong, N.D. Facile Synthesis of Ultrafine Gd_2O_3 Nanoparticles by Polyol Microwave Method. *J. Electron. Mater.* **2017**, *46*, 3484–3490. [CrossRef]
12. Lechevallier, S.; Hammer, P.; Caiut, J.M.A.; Mazeres, S.; Mauricot, R.; Verelst, M.; Dexpert, H.; Ribeiro, S.J.L.; Dexpert-Ghys, J. APTES-Modified $RE_2O_3:Eu_{3+}$ Luminescent Beads: Structure and Properties. *Langmuir* **2012**, *28*, 3962–3971. [CrossRef] [PubMed]
13. Tamrakar, R.K.; Bisen, D.P.; Upadhyay, K.; Sahu, I.P. Upconversion and Colour Tunability of $Gd_2O_3:Er^{3+}$ Phosphor Prepared by Combustion Synthesis Method. *J. Alloys Compd.* **2016**, *655*, 423–432. [CrossRef]
14. Hasani, M.; Sarabadani, P.; Hashemizadeh Aghda, A. Synthesis and Characterization of $Gd_2O_2S:Tb^{3+}$ Phosphor Powder for X-ray Imaging Detectors. *J. Nanostruct.* **2019**, *9*, 616–622. [CrossRef]
15. Wang, F.; Yang, B.; Liu, D.; Ma, W.; Chen, X.; Dai, Y. Influence of Vacuum upon Preparation and Luminescence of $Si4^+$ and Ti^{4+} Codoped $Gd_2O_2S:Eu$ Phosphor. *Spectrochim. Acta. A Mol. Biomol. Spectrosc.* **2014**, *126*, 46–52. [CrossRef]
16. Pandey, S.K.; Singh, S.; Mehta, S.K. Biocompatible Gadolinium Oxide Nanoparticles as Efficient Agent against Pathogenic Bacteria. *J. Colloid Interface Sci.* **2018**, *529*, 496–504. [CrossRef]
17. Zhou, C.; Wu, H.; Huang, C.; Wang, M.; Jia, N. Facile Synthesis of Single-Phase Mesoporous $Gd_2O_3:Eu$ Nanorods and Their Application for Drug Delivery and Multimodal Imaging. *Part. Part. Syst. Charact.* **2014**, *31*, 675–684. [CrossRef]
18. Das, G.K.; Anderson, D.S.; Wallis, C.D.; Carratt, S.A.; Kennedy, I.M.; Van Winkle, L.S. Novel Multi-Functional Europium-Doped Gadolinium Oxide Nanoparticle Aerosols Facilitate the Study of Deposition in the Developing Rat Lung. *Nanoscale* **2016**, *8*, 11518–11530. [CrossRef] [PubMed]
19. Berlanga, B.; Hernandez-Adame, L.; Angel-Olarte, C.; Aguilar, F.; Rosales-Mendoza, S.; Palestino, G. Optical and Biological Evaluation of Upconverting $Gd_2O_3:Tb^{3+}$/Er^{3+} Particles as Microcarriers of a Zika Virus Antigenic Peptide. *Chem. Eng. J.* **2019**, *385*, 123414. [CrossRef]
20. Hernandez-Adame, L.; Cortez-Espinosa, N.; Portales-Pérez, D.P.; Castillo, C.; Zhao, W.; Juarez, Z.N.; Hernandez, L.R.; Bach, H.; Palestino, G. Toxicity Evaluation of High-Fluorescent Rare-Earth Metal Nanoparticles for Bioimaging Applications. *J. Biomed. Mater. Res. B Appl. Biomater.* **2017**, *105*, 605–615. [CrossRef]
21. Pyngrope, D.; Singh, L.R.; Prasad, A.I.; Bora, A. Synthesis, Characterization and Comparative Luminescence Studies of Rare-Earth-Doped Gd_2O_3 Nanoparticles. *J. Mater. Eng. Perform.* **2018**, *27*, 2754–2758. [CrossRef]
22. Ansari, A.A.; Ahmad, N.; Labis, J.P. Highly Colloidal Luminescent Porous Tb-Doped Gadolinium Oxide Nanoparticles: Photophysical and Luminescent Properties. *J. Photochem. Photobiol. Chem.* **2019**, *371*, 10–16. [CrossRef]
23. Hazarika, S. Production and Optoelectronic Response of Tb^{3+} Activated Gadolinium Oxide Nanocrystalline Phosphors. *Eur. Phys. J. Appl. Phys.* **2013**, *62*, 30401–30406. [CrossRef]

24. He, S.; Zhao, X.; Tan, M.C. Synthesis of Uniform Rare Earth Doped Gd$_2$O$_2$S Sub-Micron Sized Spheres Using Gas-Aided Sulfurization and Their Optical Characteristics. *RSC Adv.* **2017**, *7*, 35738–35751. [CrossRef] [PubMed]

25. Song, Y.; You, H.; Huang, Y.; Yang, M.; Zheng, Y.; Zhang, L.; Guo, N. Highly Uniform and Monodisperse Gd$_2$O$_2$S:Ln^{3+} (Ln = Eu, Tb) Submicrospheres: Solvothermal Synthesis and Luminescence Properties. *Inorg. Chem.* **2010**, *49*, 11499–11504. [CrossRef] [PubMed]

26. Zatsepin, A.; Kuznetsova, Y. Down-Conversion of UV Radiation in Erbium-Doped Gadolinium Oxide Nanoparticles. *Appl. Mater. Today* **2018**, *12*, 34–42. [CrossRef]

27. Goldys, E.M.; Drozdowicz-Tomsia, K.; Jinjun, S.; Dosev, D.; Kennedy, I.M.; Yatsunenko, S.; Godlewski, M. Optical Characterization of Eu-Doped and Undoped Gd$_2$O$_3$ Nanoparticles Synthesized by the Hydrogen Flame Pyrolysis Method. *J. Am. Chem. Soc.* **2006**, *128*, 14498–14505. [CrossRef]

28. Wu, Y.; Xu, X.; Li, Q.; Yang, R.; Ding, H.; Xiao, Q. Synthesis of Bifunctional Gd$_2$O$_3$:Eu^{3+} Nanocrystals and Their Applications in Biomedical Imaging. *J. Rare Earths* **2015**, *33*, 529–534. [CrossRef]

29. Gai, S.; Yang, P.; Wang, D.; Li, C.; Niu, N.; He, F.; Li, X. Monodisperse Gd$_2$O$_3$:Ln (Ln = Eu^{3+}, Tb^{3+}, Dy^{3+}, Sm^{3+}, Yb^{3+}/Er^{3+}, Yb^{3+}/Tm^{3+}, and Yb^{3+}/Ho^{3+}) Nanocrystals with Tunable Size and Multicolor Luminescent Properties. *CrystEngComm* **2011**, *13*, 5480–5487. [CrossRef]

30. Upadhyay, K.; Tamrakar, R.K.; Bisen, D.P.; Sahu, I.P.; Sahu, M. Enhancement of Photoluminescence Behavior of Gd$_2$O$_3$:Er^{3+} Phosphor by Alkali Metal. *Optik* **2016**, *127*, 3693–3697. [CrossRef]

31. Gordon, W.O.; Carter, J.A.; Tissue, B.M. Long-Lifetime Luminescence of Lanthanide-Doped Gadolinium Oxide Nanoparticles for Immunoassays. *J. Lumin.* **2004**, *108*, 339–342. [CrossRef]

32. Rosa, I. Synthesis, Structural and Photophysical Properties of Gd$_2$O$_3$:Eu^{3+} Nanostructures Prepared by a Microwave Sintering Process. *Adv. Chem. Eng. Sci.* **2014**, *4*, 374.

33. Chavez, D.; Contreras, O.; Hirata, G. Synthesis and Upconversion Luminescence of Nanoparticles Y$_2$O$_3$ and Gd$_2$O$_3$ Co-Doped with Yb^{3+} and Er^{3+}. *Nanomater. Nanotechnol.* **2016**, *6*, 7. [CrossRef]

34. Wu, M.; Guan, G.; Yao, B.; Teng, C.-P.; Liu, S.; Tee, S.Y.; Ong, B.C.; Dong, Z.; Han, M.-Y. Upconversion Luminescence of Gd$_2$O$_3$:Ln^{3+} Nanorods for White Emission and Cellular Imaging via Surface Charging and Crystallinity Control. *ACS Appl. Nano Mater.* **2019**, *2*, 1421–1430. [CrossRef]

35. Jadhav, A.; Oh, J.H.; Park, S.; Choi, H.; Moon, B.; Choi, B.; Jang, K.; Jeong, J.; Yi, S.; Hwan, K. Enhanced down and Upconversion Emission for Li$^+$ Co-Doped Gd$_2$O$_3$:Er^{3+} Nanostructures. *Curr. Appl. Phys.* **2016**, *16*. [CrossRef]

36. Haoyue, H.; Zhang, X.; Wang, Y.; Liang, L. Up-Conversion Luminescence of Yb^{3+}/Er^{3+} Doped Gd$_2$O$_3$ Phosphors for Optical Temperature Sensing in Green and Red Regions. *Opt. Commun.* **2019**, *452*, 387–394. [CrossRef]

37. Zhao, X.; Suo, H.; Zhang, Z.; Guo, C. Cross-Relaxation and Non-Steady-State Processes Induced up-Conversion Color Modulation in Gd$_2$O$_3$: Ln^{3+}/Er^{3+} (Ln = Tm, Ho). *Dyes Pigments* **2018**, *151*, 335–341. [CrossRef]

38. Liu, Z.; Pu, F.; Huang, S.; Yuan, Q.; Ren, J.; Qu, X. Long-Circulating Gd$_2$O$_3$:Yb^{3+}, Er^{3+} up-Conversion Nanoprobes as High-Performance Contrast Agents for Multi-Modality Imaging. *Biomaterials* **2012**, *34*, 1712–1721. [CrossRef]

39. Dutta, R.K.; Pandey, A.C. Fluorescent Magnetic Gadolinium Oxide Nanoparticles for Biomedical Applications. *Nanosci. Technol.* **2015**, *2*, 1–6.

40. Das, G.K.; Heng, B.C.; Ng, S.-C.; White, T.; Loo, J.S.C.; D'Silva, L.; Padmanabhan, P.; Bhakoo, K.K.; Selvan, S.T.; Tan, T.T.Y. Gadolinium Oxide Ultranarrow Nanorods as Multimodal Contrast Agents for Optical and Magnetic Resonance Imaging. *Langmuir* **2010**, *26*, 8959–8965. [CrossRef]

41. Jia, G.; Zhang, C.; Ding, S.; Wang, L. General Synthesis Route to Fabricate Uniform Upconversion Luminescent Gadolinium Oxide Hollow Spheres. *J. Nanosci. Nanotechnol.* **2011**, *11*, 6875–6879. [CrossRef]

42. Liu, J.; Tian, X.; Chen, H.; Shao, Y.; Yang, G.; Chen, D. Near-Infrared to Visible and near-Infrared Upconversion of Monoclinic Gd$_2$O$_3$:Yb^{3+}/Tm^{3+} Nanoparticles Prepared by Laser Ablation in Liquid for Fluorescence Imaging. *Appl. Surf. Sci.* **2015**, *348*, 60–65. [CrossRef]

43. Antić, Ž.; Lojpur, V.; Nikolić, M.G.; Đorđević, V.; Ahrenkiel, P.S.; Dramićanin, M.D. Strong Emission via Up-Conversion of Gd$_2$O$_3$:Yb^{3+}, Ho^{3+} Nanopowders Co-Doped with Alkali Metals Ions. *J. Lumin.* **2014**, *145*, 466–472. [CrossRef]

44. Liu, J.; Huang, L.; Tian, X.; Chen, X.; Shao, Y.; Xie, F.; Chen, D.; Li, L. Magnetic and Fluorescent Gd$_2$O$_3$:Yb^{3+}/Ln^{3+} Nanoparticles for Simultaneous Upconversion Luminescence/MR Dual Modal Imaging and NIR-Induced Photodynamic Therapy. *Int. J. Nanomed.* **2016**, *12*, 1–14. [CrossRef]

45. Osseni, S.A.; Lechevallier, S.; Verelst, M.; Perriat, P.; Dexpert-Ghys, J.; Neumeyer, D.; Garcia, R.; Mayer, F.; Djanashvili, K.; Peters, J.A.; et al. Gadolinium Oxysulfide Nanoparticles as Multimodal Imaging Agents for T2-Weighted MR, X-ray Tomography and Photoluminescence. *Nanoscale* **2014**, *6*, 555–564. [CrossRef]

46. Qian, B.; Wang, D.; Wang, H.; Zou, H.; Song, Y.; Zhou, X.; Sheng, Y. Solvothermal Synthesis of Columnar Gd2O2S:Eu3+ and a Comparative Study with Columnar Gd$_2$O$_3$:Eu^{3+}. *J. Am. Ceram. Soc.* **2020**, *103*, 356–366. [CrossRef]

47. Fischer, S.; Martín-Rodríguez, R.; Fröhlich, B.; Krämer, K.W.; Meijerink, A.; Goldschmidt, J.C. Upconversion Quantum Yield of Er^{3+}-Doped β-NaYF$_4$ and Gd$_2$O$_2$S: The Effects of Host Lattice, Er^{3+} Doping, and Excitation Spectrum Bandwidth. *J. Lumin.* **2014**, *153*, 281–287. [CrossRef]

48. Ai, F.; Goel, S.; Zhan, Y.; Valdovinos, H.F.; Chen, F.; Barnhart, T.E.; Cai, W. Intrinsically (89)Zr-Labeled Gd$_2$O$_2$S:Eu Nanophosphors with High in Vivo Stability for Dual-Modality Imaging. *Am. J. Transl. Res.* **2016**, *8*, 5591–5600.

49. Lin, S.-L.; Liu, T.-Y.; Lo, C.-L.; Wang, B.-S.; Lee, Y.-J.; Lin, K.-Y.; Chang, C.A. Synthesis, Surface Modification, and Photophysical Studies of $Ln_2O_2S:Ln^{3'+}$ (Ln = Gd, Tb, Eu; Ln' = Tb and/ or Eu) Nanoparticles for Luminescence Bioimaging. *J. Lumin.* **2016**, *175*, 165–175. [CrossRef]

50. Rahim, S.; Ayob, M.T.M.; Hasim, M.H.; Abdul Rahman, I.; Radiman, S. Physical and Optical Studies of $Gd_2O_2S:Eu^{3+}$ Nanophosphors by Microwave Irradiation and γ-Irradiation Methods. *Luminescence* **2019**, *34*, 699–706. [CrossRef] [PubMed]

51. Li, W.; Kou, H.; Zhang, W.; Ge, L.; Pan, H.; Hu, Z.; Zhang, Y. Preparation and Characterization of Multilayer $Gd_2O_2S:Tb$ Phosphor Screen for X-ray Detection Application. *Int. J. Appl. Ceram. Technol.* **2020**, *17*, 1440–1444. [CrossRef]

52. Guleria, A.; Pranjali, P.; Meher, M.K.; Chaturvedi, A.; Chakraborti, S.; Raj, R.; Poluri, K.M.; Kumar, D. Effect of Polyol Chain Length on Proton Relaxivity of Gadolinium Oxide Nanoparticles for Enhanced Magnetic Resonance Imaging Contrast. *J. Phys. Chem. C* **2019**, *123*, 18061–18070. [CrossRef]

53. Einarsrud, M.-A.; Grande, T. 1D Oxide Nanostructures from Chemical Solutions. *Chem. Soc. Rev.* **2014**, *43*, 2187–2199. [CrossRef]

54. Yang, J.; Li, C.; Cheng, Z.; Zhang, X.; Quan, Z.; Zhang, C.; Lin, J. Size-Tailored Synthesis and Luminescent Properties of One-Dimensional $Gd_2O_3:Eu^{3+}$ Nanorods and Microrods. *J. Phys. Chem. C* **2007**, *111*, 18148–18154. [CrossRef]

55. Yi, Z.; Wen, B.; Qian, C.; Wang, H.; Rao, L.; Liu, H.; Zeng, S. Intense Red Upconversion Emission and Shape Controlled Synthesis of $Gd_2O_3:Yb/Er$ Nanocrystals. *Adv. Condens. Matter Phys.* **2013**, *2013*, 1–5. [CrossRef]

56. Wang, Z.; Wang, P.; Zhong, J.; Liang, H.; Wang, J. Phase Transformation and Spectroscopic Adjustment of $Gd_2O_3:Eu^{3+}$ Synthesized by Hydrothermal Method. *J. Lumin.* **2014**, *152*, 172–175. [CrossRef]

57. Zhou, L.; Gu, Z.; Liu, X.; Yin, W.; Tian, G.; Yan, L.; Jin, S.; Ren, W.; Xing, G.; Li, W.; et al. Size-Tunable Synthesis of Lanthanide-Doped Gd_2O_3 Nanoparticles and Their Applications for Optical and Magnetic Resonance Imaging. *J. Mater. Chem.* **2012**, *22*, 966–974. [CrossRef]

58. Xing, G.; Guo, Q.; Liu, Q.; Li, Y.; Wang, Y.; Wu, Z.; Wu, G. Highly Uniform $Gd(OH)_3$ and $Gd_2O_3:Eu^{3+}$ Hexagram-like Microcrystals: Glucose-Assisted Hydrothermal Synthesis, Growth Mechanism and Luminescence Property. *Ceram. Int.* **2014**, *40*, 6569–6577. [CrossRef]

59. Peng, L.; Han, T.; Chen, H.; Zhang, T. Spectroscopic Properties of $Gd_2O_3:Dy^{3+}$ Nanocrystals. *J. Rare Earths* **2013**, *31*, 235–240. [CrossRef]

60. Park, S.J.; Park, J.Y.; Yang, H.K. Multi Modality of Hollow Tube $Gd_2O_3:Eu^{3+}$ Nanoparticles by Using Nonpolar Solvent. *J. Alloys Compd.* **2017**, *725*, 807–817. [CrossRef]

61. Shaporev, A.; Sokolov, M.; Vanetsev, A.; Kulakova, A.; Tretyakov, Y. Solvothermal Synthesis of Colloidal Solutions of $Gd_2O_3:Eu$ Luminescent Nanoplates. *Dokl. Chem.* **2011**, *441*, 321. [CrossRef]

62. Zhang, N.; Yi, R.; Zhou, L.; Gao, G.; Shi, R.; Qiu, G.; Liu, X. Lanthanide Hydroxide Nanorods and Their Thermal Decomposition to Lanthanide Oxide Nanorods. *Mater. Chem. Phys.* **2009**, *114*, 160–167. [CrossRef]

63. Xia, T.; Wang, J.; Lin, N.; Huo, L.; Zhao, H.; Mountrichas, G. Template-Free Synthesis, Growth Mechanism and Photoluminescent Properties of $Ln(OH)_3$ and Ln_2O_3 Nanorods (Ln: Lanthanide Ion). *J. Alloys Compd.* **2010**, *507*, 245–252. [CrossRef]

64. Chaudhary, S.; Kumar, S.; Kumar, S.; Chaudhary, G.R.; Mehta, S.K.; Umar, A. Ethylene Glycol Functionalized Gadolinium Oxide Nanoparticles as a Potential Electrochemical Sensing Platform for Hydrazine and P-Nitrophenol. *Coatings* **2019**, *9*, 633. [CrossRef]

65. Wu, C.; Cai, R.; Zhao, T.; Wu, L.; Zhang, L.; Jin, J.; Xu, L.; Li, P.; Li, T.; Zhang, M.; et al. Hyaluronic Acid-Functionalized Gadolinium Oxide Nanoparticles for Magnetic Resonance Imaging-Guided Radiotherapy of Tumors. *Nanoscale Res. Lett.* **2020**, *15*, 94. [CrossRef] [PubMed]

66. Surendra, T.V.; Roopan, S.M.; Khan, M.R. Biogenic Approach to Synthesize Rod Shaped Gd_2O_3 Nanoparticles and Its Optimization Using Response Surface Methodology-Box–Behnken Design Model. *Biotechnol. Prog.* **2019**, *35*, e2823. [CrossRef] [PubMed]

67. Vahdatkhah, P.; Madaah Hosseini, H.R.; Khodaei, A.; Montazerabadi, A.R.; Irajirad, R.; Oghabian, M.A.; Delavari, H.H. Rapid Microwave-Assisted Synthesis of PVP-Coated Ultrasmall Gadolinium Oxide Nanoparticles for Magnetic Resonance Imaging. *Chem. Phys.* **2015**, *453–454*, 35–41. [CrossRef]

68. Zhang, W.; Martinelli, J.; Mayer, F.; Bonnet, C.S.; Szeremeta, F.; Djanashvili, K. Molecular Architecture Control in Synthesis of Spherical Ln-Containing Nanoparticles. *RSC Adv.* **2015**, *5*, 69861–69869. [CrossRef]

69. Khan, S.A.; Gambhir, S.; Ahmad, A. Extracellular Biosynthesis of Gadolinium Oxide (Gd_2O_3) Nanoparticles, Their Biodistribution and Bioconjugation with the Chemically Modified Anticancer Drug Taxol. *Beilstein J. Nanotechnol.* **2014**, *5*, 249–257. [CrossRef]

70. Dědková, K.; Kuzníková, Ľ.; Pavelek, L.; Matějová, K.; Kupková, J.; Barabaszová, K.Č.; Váňa, R.; Burda, J.; Vlček, J.; Cvejn, D.; et al. Daylight Induced Antibacterial Activity of Gadolinium Oxide, Samarium Oxide and Erbium Oxide Nanoparticles and Their Aquatic Toxicity. *Mater. Chem. Phys.* **2017**, *197*, 226–235. [CrossRef]

71. Tamrakar, R.K.; Bisen, D.; Brahme, N. Combustion Synthesis and Upconversion Luminescence Properties of Er^{3+}, Yb^{3+} Doped Gadolinium Oxide Nanophosphor. *Recent Res. Sci. Technol.* **2012**, *4*, 70–72.

72. Jayasimhadri, M.; Ratnam, B.V.; Jang, K.; Lee, H.S.; Chen, B.; Yi, S.-S.; Jeong, J.-H.; Rama Moorthy, L. Combustion Synthesis and Luminescent Properties of Nano and Submicrometer-Size $Gd_2O_3:Dy^{3+}$ Phosphors for White LEDs. *Int. J. Appl. Ceram. Technol.* **2011**, *8*, 709–717. [CrossRef]

73. Tamrakar, R.; Bisen, D.P.; Upadhyay, K.; Brahme, N. Effect of Fuel on Structural and Optical Characterization of $Gd_2O_3:Er^{3+}$ Phosphor. *J. Lumin. Appl.* **2014**, *1*, 23–29. [CrossRef]

74. Jain, A.; Hirata, G.A.; Farías, M.H.; Castillón, F.F. Synthesis and Characterization of (3-Aminopropyl)Trimethoxy-Silane (APTMS) Functionalized $Gd_2O_3:Eu^{3+}$ red Phosphor with Enhanced Quantum Yield. *Nanotechnology* **2015**, *27*, 065601. [CrossRef]

75. Matijević, E.; Hsu, W.P. Preparation and Properties of Monodispersed Colloidal Particles of Lanthanide Compounds: I. Gadolinium, Europium, Terbium, Samarium, and Cerium(III). *J. Colloid Interface Sci.* **1987**, *118*, 506–523. [CrossRef]

76. Li, D.; Qin, W.; Aidilibike, T.; Zhang, P.; Liu, S.; Wang, L.; Li, S. Enhanced Upconversion Emission and Magnetization in Yb^{3+}-Er^{3+}/Ho^{3+} Codoped Gd_2O_3 Nanocrystals by Introducing Zn^{2+} Ions. *J. Alloys Compd.* **2016**, *675*, 31–36. [CrossRef]

77. Hernández-Adame, L.; Méndez-Blas, A.; Ruiz-García, J.; Vega-Acosta, J.R.; Medellín-Rodríguez, F.J.; Palestino, G. Synthesis, Characterization, and Photoluminescence Properties of Gd:Tb Oxysulfide Colloidal Particles. *Chem. Eng. J.* **2014**, *258*, 136–145. [CrossRef]

78. Lechevallier, S.; Lecante, P.; Mauricot, R.; Dexpert, H.; Dexpert-Ghys, J.; Kong, H.-K.; Law, G.-L.; Wong, K.-L. Gadolinium−Europium Carbonate Particles: Controlled Precipitation for Luminescent Biolabeling. *Chem. Mater.* **2010**, *22*, 6153–6161. [CrossRef]

79. Cichos, J.; Karbowiak, M.; Hreniak, D.; Stręk, W. Synthesis and Characterization of Monodisperse Eu^{3+} Doped Gadolinium Oxysulfide Nanocrystals. *J. Rare Earths* **2016**, *34*, 850–856. [CrossRef]

80. Lian, J.; Qin, H.; Liang, P.; Wang, B.; Liu, F. Controllable Synthesis and Photoluminescence Properties of $Gd_2O_2S:Pr^{3+}$ Microspheres Using an Urea-Ammonium Sulfate (UAS) System. *Ceram. Int.* **2015**, *41*, 2990–2998. [CrossRef]

81. Thirumalai, J.; Chandramohan, R.; Vijayan, T.A. Synthesis, Characterization and Formation Mechanism of Monodispersed $Gd_2O_2S:Eu^{3+}$ Nanocrystals. *J. Mater. Sci. Mater. Electron.* **2011**, *22*, 936–943. [CrossRef]

82. Luo, M.; Xu, L.; Xia, J.; Zhao, H.; Du, Y.; Lei, B. Synthesis of Porous Gadolinium Oxide Nanosheets for Cancer Therapy and Magnetic Resonance Imaging. *Mater. Lett.* **2020**, *265*, 127375. [CrossRef]

83. Singh, G.; McDonagh, B.H.; Hak, S.; Peddis, D.; Bandopadhyay, S.; Sandvig, I.; Sandvig, A.; Glomm, W.R. Synthesis of Gadolinium Oxide Nanodisks and Gadolinium Doped Iron Oxide Nanoparticles for MR Contrast Agents. *J. Mater. Chem. B* **2017**, *5*, 418–422. [CrossRef] [PubMed]

84. Santelli, J.; Lechevallier, S.; Calise, D.; Marsal, D.; Siegfried, A.; Vincent, M.; Martinez, C.; Cussac, D.; Mauricot, R.; Verelst, M. Multimodal Gadolinium Oxysulfide Nanoparticles for Bioimaging: A Comprehensive Biodistribution, Elimination and Toxicological Study. *Acta Biomater.* **2020**, *108*, 261–272. [CrossRef] [PubMed]

85. Hernandez-Adame, L.; Palestino, G.; Meza, O.; Hernandez-Adame, P.L.; Vega-Carrillo, H.R.; Sarhid, I. Effect of Tb^{3+} Concentration in the Visible Emission of Terbium-Doped Gadolinium Oxysulfide Microspheres. *Solid State Sci.* **2018**, *84*, 8–14. [CrossRef]

86. Chen, J.; Song, Y.; Li, D.; Ma, Q.; Dong, X.; Yu, W.; Wang, X.; Yang, Y.; Wang, J.; Liu, G. Investigating Efficient Energy Transfer in Novel Strategy-Obtained $Gd_2O_2S:Dy^{3+}$, Eu^{3+} Nanofibers Endowed with White Emitting and Magnetic Dual-Functionality. *J. Lumin.* **2019**, *206*, 509–517. [CrossRef]

87. Thirumalai, J.; Chandramohan, R.; Divakar, R.; Mohandas, E.; Sekar, M.; Parameswaran, P. Eu^{3+} Doped Gadolinium Oxysulfide (Gd_2O_2S) Nanostructures—Synthesis and Optical and Electronic Properties. *Nanotechnology* **2008**, *19*, 395703. [CrossRef] [PubMed]

88. Thirumalai, J.; Chandramohan, R.; Valanarasu, S.; Vijayan, T.A.; Somasundaram, R.M.; Mahalingam, T.; Srikumar, S.R. Shape-Selective Synthesis and Opto-Electronic Properties of Eu^{3+}-Doped Gadolinium Oxysulfide Nanostructures. *J. Mater. Sci.* **2009**, *44*, 3889–3899. [CrossRef]

89. Kang, M.-K.; Lee, G.H.; Jung, K.-H.; Jung, J.-C.; Kim, H.-K.; Kim, Y.-H.; Lee, J.; Ryeom, H.-K.; Kim, T.-J.; Chang, Y. Gadolinium Nanoparticles Conjugated with Therapeutic Bifunctional Chelate as a Potential T 1 Theranostic Magnetic Resonance Imaging Agent. *J. Biomed. Nanotechnol.* **2016**, *12*, 894–908. [CrossRef]

90. Podgórna, K.; Szczepanowicz, K.; Piotrowski, M.; Gajdošová, M.; Štěpánek, F.; Warszyński, P. Gadolinium Alginate Nanogels for Theranostic Applications. *Colloids Surf. B Biointerfaces* **2017**, *153*, 183–189. [CrossRef]

91. Ho, S.L.; Choi, G.; Yue, H.; Kim, H.K.; Jung, K.H.; Park, J.A.; Kim, M.H.; Lee, Y.J.; Kim, J.Y.; Miao, X.; et al. In Vivo Neutron Capture Therapy of Cancer Using Ultrasmall Gadolinium Oxide Nanoparticles with Cancer-Targeting Ability. *RSC Adv.* **2020**, *10*, 865–874. [CrossRef]

92. Shen, Z.; Liu, T.; Yang, Z.; Zhou, Z.; Tang, W.; Fan, W.; Liu, Y.; Mu, J.; Li, L.; Bregadze, V.I.; et al. Small-Sized Gadolinium Oxide Based Nanoparticles for High-Efficiency Theranostics of Orthotopic Glioblastoma. *Biomaterials* **2020**, *235*, 119783. [CrossRef] [PubMed]

93. Sui, Y.; Li, Y.; Li, Y.; Jin, H.; Zheng, Y.; Huang, W.; Chen, S. Tumor-Specific Design of PEGylated Gadolinium-Based Nanoscale Particles: Facile Synthesis, Characterization, and Improved Magnetic Resonance Imaging of Metastasis Lung Cancer. *J. Photochem. Photobiol. B* **2020**, *202*, 111669. [CrossRef] [PubMed]

94. Yue, H.; Marasini, S.; Ahmad, M.Y.; Ho, S.L.; Cha, H.; Liu, S.; Jang, Y.J.; Tegafaw, T.; Ghazanfari, A.; Miao, X.; et al. Carbon-Coated Ultrasmall Gadolinium Oxide (Gd_2O_3@C) Nanoparticles: Application to Magnetic Resonance Imaging and Fluorescence Properties. *Colloids Surf. Physicochem. Eng. Asp.* **2020**, *586*, 124261. [CrossRef]

95. Jamil, M.Z.A.M.; Mohamed, F.; Rosli, N.R.A.M.; Rahman, I.A.; Idris, M.I.; Bradley, D.A.; Nor, M.M.; Mustafa, S.N.M. Effect of Gamma Irradiation on Magnetic Gadolinium Oxide Nanoparticles Coated with Chitosan (GdNPs-Cs) as Contrast Agent in Magnetic Resonance Imaging. *Radiat. Phys. Chem.* **2019**, *165*, 108407. [CrossRef]

96. Mortezazadeh, T.; Gholibegloo, E.; Alam, N.R.; Dehghani, S.; Haghgoo, S.; Ghanaati, H.; Khoobi, M. Gadolinium (III) Oxide Nanoparticles Coated with Folic Acid-Functionalized Poly(β-Cyclodextrin-Co-Pentetic Acid) as a Biocompatible Targeted Nano-Contrast Agent for Cancer Diagnostic: In Vitro and in Vivo Studies. *Magn. Reson. Mater. Phys. Biol. Med.* **2019**, *32*, 487–500. [CrossRef]

97. Mortezazadeh, T.; Gholibegloo, E.; Khoobi, M.; Alam, N.R.; Haghgoo, S.; Mesbahi, A. In Vitro and in Vivo Characteristics of Doxorubicin-Loaded Cyclodextrine-Based Polyester Modified Gadolinium Oxide Nanoparticles: A Versatile Targeted Theranostic System for Tumour Chemotherapy and Molecular Resonance Imaging. *J. Drug Target.* **2020**, *28*, 533–546. [CrossRef]

98. Kumar, S.; Meena, V.K.; Hazari, P.P.; Sharma, S.K.; Sharma, R.K. Rose Bengal Attached and Dextran Coated Gadolinium Oxide Nanoparticles for Potential Diagnostic Imaging Applications. *Eur. J. Pharm. Sci.* **2018**, *117*, 362–370. [CrossRef] [PubMed]

99. Santelli, J.; Lechevallier, S.; Baaziz, H.; Vincent, M.; Martinez, C.; Mauricot, R.; Parini, A.; Verelst, M.; Cussac, D. Multimodal Gadolinium Oxysulfide Nanoparticles: A Versatile Contrast Agent for Mesenchymal Stem Cell Labeling. *Nanoscale* **2018**, *10*, 16775–16786. [CrossRef]

100. Osseni, S.A.; Lechevallier, S.; Verelst, M.; Dujardin, C.; Dexpert-Ghys, J.; Neumeyer, D.; Leclercq, M.; Baaziz, H.; Cussac, D.; Santran, V.; et al. New Nanoplatform Based on $Gd_2O_2S:Eu^{3+}$ Core: Synthesis, Characterization and Use for in Vitro Bio-Labelling. *J. Mater. Chem.* **2011**, *21*, 18365–18372. [CrossRef]

101. Stöber, W.; Fink, A.; Bohn, E. Controlled Growth of Monodisperse Silica Spheres in the Micron Size Range. *J. Colloid Interface Sci.* **1968**, *26*, 62–69. [CrossRef]

102. Guo, X.; Deng, Y.; Gu, D.; Che, R.; Zhao, D. Synthesis and Microwave Absorption of Uniform Hematite Nanoparticles and Their Core-Shell Mesoporous Silica Nanocomposites. *J. Mater. Chem.* **2009**, *19*, 6706–6712. [CrossRef]

103. Liu, Z.; Liu, X.; Yuan, Q.; Dong, K.; Jiang, L.; Li, Z.; Ren, J.; Qu, X. Hybrid Mesoporous Gadolinium Oxide Nanorods: A Platform for Multimodal Imaging and Enhanced Insoluble Anticancer Drug Delivery with Low Systemic Toxicity. *J. Mater. Chem.* **2012**, *22*, 14982–14990. [CrossRef]

104. Bouzigues, C.; Gacoin, T.; Alexandrou, A. Biological Applications of Rare-Earth Based Nanoparticles. *ACS Nano* **2011**, *5*, 8488–8505. [CrossRef]

105. Fan, Q.; Cui, X.; Guo, H.; Xu, Y.; Zhang, G.; Peng, B. Application of Rare Earth-Doped Nanoparticles in Biological Imaging and Tumor Treatment. *J. Biomater. Appl.* **2020**, *35*, 237–263. [CrossRef]

106. Bridot, J.-L.; Faure, A.-C.; Laurent, S.; Rivière, C.; Billotey, C.; Hiba, B.; Janier, M.; Josserand, V.; Coll, J.-L.; Vander Elst, L.; et al. Hybrid Gadolinium Oxide Nanoparticles: Multimodal Contrast Agents for in Vivo Imaging. *J. Am. Chem. Soc.* **2007**, *129*, 5076–5084. [CrossRef]

107. Maalej, N.M.; Qurashi, A.; Assadi, A.A.; Maalej, R.; Shaikh, M.N.; Ilyas, M.; Gondal, M.A. Synthesis of $Gd_2O_3:Eu$ Nanoplatelets for MRI and Fluorescence Imaging. *Nanoscale Res. Lett.* **2015**, *10*, 215. [CrossRef]

108. Faucher, L.; Tremblay, M.; Lagueux, J.; Gossuin, Y.; Fortin, M.-A. Rapid Synthesis of PEGylated Ultrasmall Gadolinium Oxide Nanoparticles for Cell Labeling and Tracking with MRI. *ACS Appl. Mater. Interfaces* **2012**, *4*, 4506–4515. [CrossRef] [PubMed]

109. Nichkova, M.; Dosev, D.; Perron, R.; Gee, S.J.; Hammock, B.D.; Kennedy, I.M. Eu3+-Doped Gd_2O_3 Nanoparticles as Reporters for Optical Detection and Visualization of Antibodies Patterned by Microcontact Printing. *Anal. Bioanal. Chem.* **2006**, *384*, 631–637. [CrossRef] [PubMed]

110. Dosev, D.; Nichkova, M.; Liu, M.; Guo, B.; Liu, G.; Xia, Y.; Hammock, B.D.; Kennedy, I.M. Application of Fluorescent $Eu:Gd_2O_3$ Nanoparticles to the Visualization of Protein Micropatterns. In Proceedings of the Imaging, Manipulation, and Analysis of Biomolecules and Cells: Fundamentals and Applications III, San Jose, CA, USA, 24–27 January 2005; International Society for Optics and Photonics: Bellingham, WA, USA, 2005; 5699, pp. 473–481.

111. Fang, J.; Chandrasekharan, P.; Liu, X.-L.; Yang, Y.; Lv, Y.-B.; Yang, C.-T.; Ding, J. Manipulating the Surface Coating of Ultra-Small Gd_2O_3 Nanoparticles for Improved T1-Weighted MR Imaging. *Biomaterials* **2014**, *35*, 1636–1642. [CrossRef]

112. Mekuria, S.L.; Debele, T.A.; Tsai, H.-C. Encapsulation of Gadolinium Oxide Nanoparticle (Gd_2O_3) Contrasting Agents in PAMAM Dendrimer Templates for Enhanced Magnetic Resonance Imaging in Vivo. *ACS Appl. Mater. Interfaces* **2017**, *9*, 6782–6795. [CrossRef] [PubMed]

113. Mastrogiacomo, S.; Kownacka, A.E.; Dou, W.; Burke, B.P.; de Rosales, R.T.M.; Heerschap, A.; Jansen, J.A.; Archibald, S.J.; Walboomers, X.F. Bisphosphonate Functionalized Gadolinium Oxide Nanoparticles Allow Long-Term MRI/CT Multimodal Imaging of Calcium Phosphate Bone Cement. *Adv. Healthc. Mater.* **2018**, *7*, 1800202. [CrossRef]

114. Rosticher, C.; Viana, B.; Fortin, M.-A.; Lagueux, J.; Faucher, L.; Chanéac, C. Gadolinium Oxysulfide Nanoprobes with Both Persistent Luminescent and Magnetic Properties for Multimodal Imaging. *RSC Adv.* **2016**, *6*, 55472–55478. [CrossRef]

115. Pandey, S.K.; Singh, S.; Mehta, S.K. Ultrasonication Assisted Fabrication of L-Lysine Functionalized Gadolinium Oxide Nanoparticles and Its Biological Acceptability. *Ultrason. Sonochem.* **2018**, *49*, 53–62. [CrossRef] [PubMed]

116. Yang, H.-W.; Huang, C.-Y.; Lin, C.-W.; Liu, H.-L.; Huang, C.-W.; Liao, S.-S.; Chen, P.-Y.; Lu, Y.-J.; Wei, K.-C.; Ma, C.-C.M. Gadolinium-Functionalized Nanographene Oxide for Combined Drug and MicroRNA Delivery and Magnetic Resonance Imaging. *Biomaterials* **2014**, *35*, 6534–6542. [CrossRef]

117. Yoo, S.S.; Razzak, R.; Bédard, E.; Guo, L.; Shaw, A.R.; Moore, R.B.; Roa, W.H. Layered Gadolinium-Based Nanoparticle as a Novel Delivery Platform for MicroRNA Therapeutics. *Nanotechnology* **2014**, *25*, 425102. [CrossRef]

118. Saha, A.; Mohanta, S.C.; Deka, K.; Deb, P.; Devi, P.S. Surface-Engineered Multifunctional $Eu:Gd_2O_3$ Nanoplates for Targeted and PH-Responsive Drug Delivery and Imaging Applications. *ACS Appl. Mater. Interfaces* **2017**, *9*, 4126–4141. [CrossRef] [PubMed]

119. Xu, Z.; Gao, Y.; Huang, S.; Ma, P.; Lin, J.; Fang, J. A Luminescent and Mesoporous Core-Shell Structured $Gd_2O_3:Eu^{3+}@nSiO_2@mSiO_2$ Nanocomposite as a Drug Carrier. *Dalton Trans.* **2011**, *40*, 4846–4854. [CrossRef]

120. Abid, A.D.; Anderson, D.S.; Das, G.K.; Van Winkle, L.S.; Kennedy, I.M. Novel Lanthanide-Labeled Metal Oxide Nanoparticles Improve the Measurement of in Vivo Clearance and Translocation. *Part. Fibre Toxicol.* **2013**, *10*, 1. [CrossRef] [PubMed]

121. Li, F.; Li, Z.; Jin, X.; Liu, Y.; Zhang, P.; Li, P.; Shen, Z.; Wu, A.; Chen, W.; Li, Q. Ultra-Small Gadolinium Oxide Nanocrystal Sensitization of Non-Small-Cell Lung Cancer Cells toward X-ray Irradiation by Promoting Cytostatic Autophagy. *Int. J. Nanomed.* **2019**, *14*, 2415–2431. [CrossRef]

122. Priya, R.; Pandey, O.P.; Dhoble, S.J. Review on the Synthesis, Structural and Photo-Physical Properties of Gd_2O_3 Phosphors for Various Luminescent Applications. *Opt. Laser Technol.* **2021**, *135*, 106663. [CrossRef]

123. Söderlind, F.; Pedersen, H.; Petoral, R.M.; Käll, P.-O.; Uvdal, K. Synthesis and Characterisation of Gd_2O_3 Nanocrystals Functionalised by Organic Acids. *J. Colloid Interface Sci.* **2005**, *288*, 140–148. [CrossRef]

124. Larquet, C.; Hourlier, D.; Nguyen, A.-M.; Torres-Pardo, A.; Gauzzi, A.; Sanchez, C.; Carenco, S. Thermal Stability of Oleate-Stabilized Gd_2O_2S Nanoplates in Inert and Oxidizing Atmospheres. *ChemNanoMat* **2019**, *5*, 539–546. [CrossRef]

125. Wang, F.; Chen, X.; Liu, D.; Yang, B.; Dai, Y. Experimental and Theoretical Study of Pure and Doped Crystals: Gd_2O_2S, Gd_2O_2S:Eu^{3+} and Gd_2O_2S:Tb^{3+}. *J. Mol. Struct.* **2012**, *1020*, 153–159. [CrossRef]

126. Chen, H.; Moore, T.; Qi, B.; Colvin, D.C.; Jelen, E.K.; Hitchcock, D.A.; He, J.; Mefford, O.T.; Gore, J.C.; Alexis, F.; et al. Monitoring PH-Triggered Drug Release from Radioluminescent Nanocapsules with X-ray Excited Optical Luminescence. *ACS Nano* **2013**, *7*, 1178–1187. [CrossRef]

127. Chen, H.; Rogalski, M.M.; Anker, J.N. Advances in Functional X-ray Imaging Techniques and Contrast Agents. *Phys. Chem. Chem. Phys.* **2012**, *14*, 13469–13486. [CrossRef]

128. Wang, F.; Wang, J.; Liu, X. Direct Evidence of a Surface Quenching Effect on Size-Dependent Luminescence of Upconversion Nanoparticles. *Angew. Chem. Int. Ed.* **2010**, *49*, 7456–7460. [CrossRef] [PubMed]

129. Chen, X.Y.; Zhuang, H.Z.; Liu, G.K.; Li, S.; Niedbala, R.S. Confinement on Energy Transfer between Luminescent Centers in Nanocrystals. *J. Appl. Phys.* **2003**, *94*, 5559–5565. [CrossRef]

130. Food and Drug Administration. *Drug Safety Communication: FDA Warns That Gadolinium-Based Contrast Agents (GBCAs) Are Retained in the Body*; Requires New Class Warnings; FDA: Silver Spring, MD, USA, 2019.

131. Byrne, H.L.; Le Duc, G.; Lux, F.; Tillement, O.; Holmes, N.M.; James, A.; Jelen, U.; Dong, B.; Liney, G.; Roberts, T.L.; et al. Enhanced MRI-Guided Radiotherapy with Gadolinium-Based Nanoparticles: Preclinical Evaluation with an MRI-Linac. *Cancer Nanotechnol.* **2020**, *11*, 9. [CrossRef]

132. Verry, C.; Sancey, L.; Dufort, S.; Duc, G.L.; Mendoza, C.; Lux, F.; Grand, S.; Arnaud, J.; Quesada, J.L.; Villa, J.; et al. Treatment of Multiple Brain Metastases Using Gadolinium Nanoparticles and Radiotherapy: NANO-RAD, a Phase I Study Protocol. *BMJ Open* **2019**, *9*, e023591. [CrossRef]